Lavas and their mantle xenoliths from intracratonic Eastern Paraguay (South America Platform) and Andean Domain, NW-Argentina: a comparative review

P. Comin-Chiaramonti · F. Lucassen · V. A. V. Girardi · A. De Min · C. B. Gomes

Abstract Protogranular spinel-peridotite mantle xenoliths and their host sodic alkaline lavas of Cretaceous to Paleogene age occur at the same latitude ≈26°S in central eastern Paraguay and Andes. Na- alkaline lavas from both regions display similar geochemical features, differing mainly by higher Rb content of the Paraguayan samples. Sr, Nd, and Pb isotope ratios are also similar with predominant trends from depleted to enriched mantle components. The mantle xenoliths are divided into two main suites, i.e. relatively low in potassium and incompatible elements, and high in potassium and incompatible elements. The suite high in potassium occurs only in Paraguay. Compositions of both suites range from lherzolite to dunite indicating variable "melt extraction". Clinopyroxenes from the xenoliths display variable trace element enrichment/depletion patterns compared with the pattern of average primitive mantle. Enrichment in LREE and Sr coupled with depletion of Nb, Ti and Zr in xenoliths from both areas are attributed to asthenospheric metasomatic fluids affecting the lithospheric mantle. Metasomatism is apparent in the sieve textures and glassy drops in clinopyroxenes, by glassy patches with associated primary carbonates in Paraguayan xenoliths. Trace element geochemistry and thermobarometric data indicate lack of interaction between xenoliths and host lavas, due to their rapid ascent. Sr and Nd isotope signatures of the Andean and Paraguayan xenoliths and host volcanic rocks plot mainly into the field of depleted mantle and show some compositional overlap. The Andean samples indicate a generally slightly more depleted mantle lithosphere. Pb isotope signatures in xenoliths and host volcanic rocks indicate the existence of a radiogenic Pb source (high U/Pb component in the source) in both areas. In spite of the distinct tectonic settings, generally compressive in the Central Andes (but extensional in a back-arc environment), and extensional in Eastern Paraguay (rifting environment in an intercratonic area), lavas and host xenoliths from both regions are similar in terms of geochemical and isotopic characteristics.

P. Comin-Chiaramonti (✉) · A. De Min
Earth Sciences Departement, Trieste University,
Via Weiss 8.,
I-34127 Trieste, Italy
e-mail: comin@univ.trieste.it

F. Lucassen
GeoForschungsZentrum Potsdam,
Telegrafenberg,
14473 Potsdam, Germany

F. Lucassen
Fachgebiet Petrologie, Technische Universität Berlin,
ACK 9 Ackerstr. 71-76,
13355 Berlin, Germany

V. A. V. Girardi · C. B. Gomes
Instituto de Geociências, USP,
Rua do Lago 562,
05508-080 São Paulo, Brazil

Introduction

Eastern Paraguay, central South America, extends over an intercratonic region (Fig. 1). It includes the westernmost region of the Early Cretaceous Paraná-Angola-Edendeka system (PAE) with the tholeiithic Paraná suites which developed during continent separation and the opening of the South Atlantic (Serra Geral Formation; Piccirillo and Melfi 1988). This area is located between the compressional Andean and extensional Atlantic systems (Fig. 1; Comin-
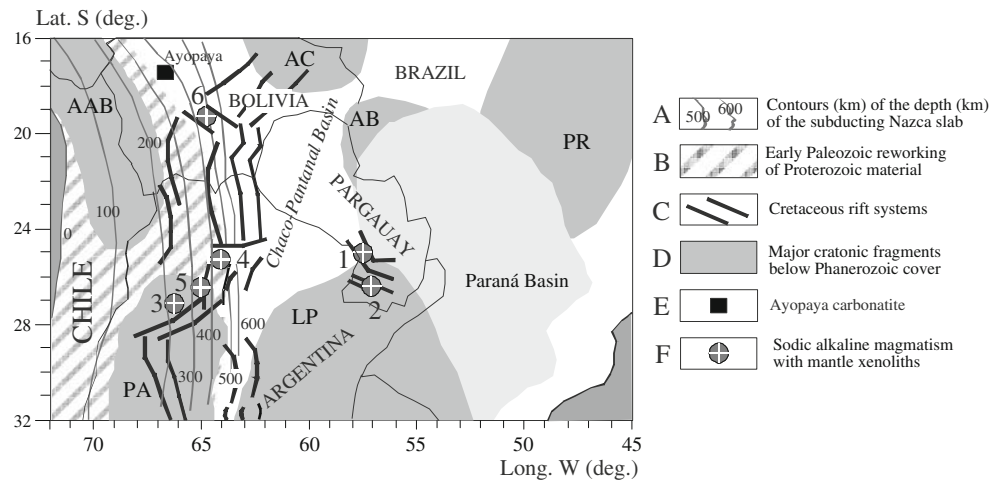
Fig. 1 Map of the studied regions (modified after Comin-Chiaramonti et al. 2007, Lucassen et al. 2007) showing: A, contours of the depth (km) of the subducting Nazca slab based on seismic data (Gudmundsson and Sambridge 1998); B, outlines of the Cretaceous rift systems (Fig. 1 of Lucassen et al. 2007 and Comin-Chiaramonti et al. 2007); C, the extension of intense early Paleozoic reworking of Proterozoic material, but the exact border to the Brazilian Craton remains unknown (Lucassen et al. 2000); D, inferred positions of major cratonic fragments below Phanerozoic cover: AAB, Arequipa-Antofalla; AC, Amazon Craton; AB,

Apa Block (Rio Apa Craton); PR, Paranapanema; LP, Rio de la Plata; PA, Pampia; D, Ayopaya carbonatite; E, localities characterized by sodic alkaline magmatism with mantle xenoliths: 1, Asunción (59 Ma) 2, Misiones (118 Ma); 3, Belén (130 Ma); 4, Las Conchas and Cadillal (100 Ma); 5, Finca del Rodeo (96 Ma); 6, Betanzos (82 Ma). Data source: Comin-Chiaramonti et al. (2007 and eclosed references); Lucassen et al. (2007 and enclosed references). Ayopaya carbonatite (100 Ma) from Schultz et al. 2004

Chiaramonti et al. 2007). The exact limit between both systems is unknown due to the development of the Chaco-Pantanal basin at the Paleogene-Neogene transition.

The Central Andes (Fig. 1) were a continental margin at least from the Neoproterozoic onwards, which was repeatedly active over extended periods in the the Early Paleozoic, Late Paleozoic and from Late Triassic — Early Jurassic onwards (e.g. Scheuber and González 1999; Taylor et al. 2005; Ramos 2008 and enclosed references). The tectonic evolution of this margin in the Neoproterozoic and during the Early Paleozoic Cambrian and Ordovician orogenies is controversely discussed as a mosaic of exotic and parauthochtonous terranes (e.g. Omarini et al. 1999; Ramos 2008), parauthochthonous terrane and a single large terrane of Laurentian origin (Rapela et al. 2007 and enclosed references), and an Andean-type orogen without collision of exotic continental fragments (e.g. Franz et al. 2006). The late Paleozoic and Mesozoic evolution of the margin proceeded without major mountain building and collision of continental fragments and included extended periods of arc magmatism under tectonic transpression or extension respectively in the Mesozoic (above references). During the Cenozoic, the Andean-type Cordillerian orogene evolved to its present form. Subduction is accepted as a first order process at this margin from Neoproterozoic onwards, regardless the concepts and details of the tectonic evolution inferred from different data sets and working groups (Scheuber and González 1999; Oliveiros et al. 2007 and enclosed references).

Extensional tectonics and rifting systems occurred in Cretaceous to Early Cenozoic times all over South America (e.g. Ramos and Aleman 2000) and triggered mantle derived intra-plate magmatism at various locations with differerent geological histories.

Around latitude 26°S mafic intra-plate magmatism bears mantle xenoliths in the cratonic Paraguayan locations (Fig. 1; e.g. Comin-Chiaramonti et al. 1991, 2001) and at the Andean margin (e.g. Lucassen et al. 2005, 2007). Host volcanic rocks (Na-alkaline, see later) and xenoliths are likely derived from the lithospheric veined mantle (Comin-Chiaramonti et al. 1991, 2001; Lucassen et al. 2005, 2007) and provide primary sources of information on the thermal and compositional state of the uppermost mantle.

This contribution reviews and discusses previous findings about the mineralogy, petrology and geochemistry of the mafic-ultramafic magmatism and associated mantle xenoliths from the Proterozoic cratonic and Phanerozoic mobile sections.

Late mesozoic to early cenozoic intra-plate magmatism

Eastern Paraguay Intra-plate magmatism of Eastern Paraguay is characterized by: **a**) potassic alkaline and alkaline-carbonatitic magmatism (Lower Cretaceous, ca. 140–126 Ma, Comin-Chiaramonti et al. 2007); **b**) Serra Geral flood tholeiites (Lower Cretaceous, 133±1.1 Ma; Renne et al. 1992), represented by high-Ti and low-Ti

variants (Piccirillo and Melfi 1988); **c**) late Lower Cretaceous (118 Ma) to Paleogene (59 Ma) sodic alkaline complexes, plugs and dykes, mafic-ultramafic in composition and with mantle xenolith (Comin-Chiaramonti et al. 1986, 2001, 2007; Velázquez et al. 2006). The latter most recent magmatism is restricted to southeast and central Paraguay, mainly to the the Misiones and Asunción provinces (Fig. 1).

Andes Pre-Cenozoic, Cretaceous rift systems, developed along the western Pacific side of the continent at NW-Argentina, mainly on a crust (intensely worked in Early Paleozoic) defining the western mobile part of the Brazilian shield (Fig. 1; Viramonte et al. 1999; Ramos and Aleman 2000; Lucassen et al. 2002, 2007). Small volume, sodic, less common potassic, alkaline magmatism with ages spanning from ~130 to 20 Ma is widespread in the hinterland of the active continental margin between 19° to 29°S (Viramonte et al. 1999; Lucassen et al. 2002, 2007). We restrict here to the locations and age groups indicated in Fig. 1, including the ~100 Ma old Ayopaya carbonatite (Schultz et al. 2004).

This magmatism locally includes mantle xenoliths (spinel facies) in Paraguay (Misiones and Asunción provinces; Fig. 1 and Comin-Chiaramonti et al. 1986, 2001) and in Andes (Las Conchas location of Fig. 1; Lucassen et al. 2005). These mantle xenoliths vary in size from a few centimetres to 45 cm and provide the unique opportunity for a direct sampling of the subcontinental mantle.

Compositional characteristics of the lavas with xenoliths and other mafic lavas

Major and trace elements

The Paraguayan Na-alkaline ultramafic lavas from Asunción and Misiones (Comin-Chiaramonti et al. 2007) are melanephelinites and subordinate ankaratrites, according to the nomenclature after De La Roche (1986; Fig. 2) and Le Maitre (1989), with mg# [MgO/(MgO + FeO) molar ratio, assuming Fe_2O_3/FeO wt% ratio = 0.21] ranging from 0.64 to 0.67 (Comin-Chiaramonti et al. 1991, 1997). The Andean Na-lavas and dykes (Lucassen et al. 2002, 2007) range from mafic to ultramafic rock-types, being ankaratrites (Finca del Rodeo, mg# 0.67), basanites (Las Conchas + Cadillal and Betanzos, mg# 0.70 and 0.59, respectively) and tephrites (Belén, mg # 0.57).

These rock-types from the Andes and Paraguay belong to the Na-alkaline suites (inset of Fig. 2), having Na_2O/K_2O ratio ranging from 2.12 to 5.85. K/Ti ranges from 0.98 to 0.54 (Paraguay) and from 0.58 to 0.32 (Andes). Their phenocryst population is characterized by olivine (1–7 vol%,
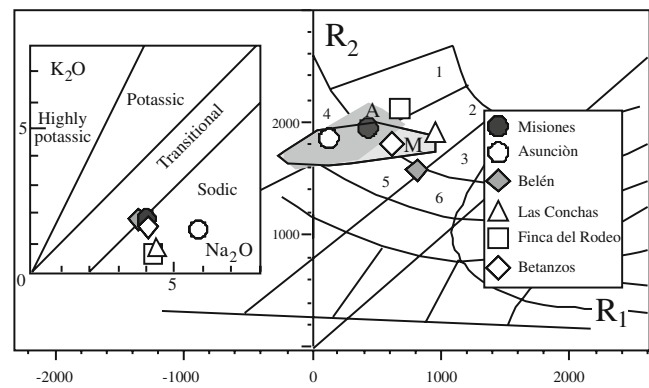
Fig. 2 Plot, following De la Roche's (1986) nomenclature, of the average rock-types (sodic-alkaline magmatism from Andes and Paraguay). R1=4Si-11(Na + K)-2(Fe + Ti), R2=6Ca + 2 Mg + Al; 1, ankaratrite; 2, basanite; 3, alkali basalt; 4, nephelinite; 5, tephrite; 6, trachybasalt. The whole compositional fields for the Misiones (M, light grey) and Asunción (A, dark grey) are also shown. **Inset**: Na_2O vs. K_2O (wt%), diagram (following Le Maitre 1989) for the averaged compositions. Data source: Comin-Chiaramonti et al. (1991); Velázquez et al. (2006 and enclosed references); Lucassen et al. (2007 and enclosed references)

Fo 89–85 mole%; 1–6 vol% microphenocrysts, Fo 82–77 mole%), clinopyroxene (1–6 vol%, mg# ~0.8), titanomagnetite (0.3–0.7 vol%, up to 38 ulv. mole%), and occasionally phlogopite, as in the Betanzos rocks (Lucassen et al. 2002). The hypocrystalline groundmass contains clinopyroxene (39–46% vol%, mg# ~0.75), olivine (3–6 vol%, Fo 74–76 mole%), titanomagnetite (4–7 vol%, up to 43% ulv.mole%), nepheline (16–21 vol%) and glass (11–25 vol%).

Trace element and REE of the Na alkaline rock-types display similar distribution patterns in Paraguay and in the Andes (Fig. 3a, b) and the major difference is the higher Rb contents of the Paraguayan rocks (K/Rb: 130 to 205 in Paraguay vs. 342–1,142 in the Andes). Moreover, two Andean localities (Finca del Rodeo and Las Conchas) have lower trace element concentrations in the Rb to Sm range. The overlapping compositions of Paraguayan and Andean magmatism are apparent, except for the Las Conchas + Cadillal basanites (mg# 0.70) that are Rb and LREE strongly depleted with respect to the other rocks. K is systematically strongly depleted in relation to neighbouring elements, whereas Ba, Nb and Ta show positive spikes. Moreover, (Eu/Eu*) is negative in Paraguay, ranging from 0.75–0.85 and near the unity in the Andean domain (1.01–1.03; Fig. 3). Melting models indicate that the Na-alkaline rocks from Paraguay and Andes were derived from liquids representing about 4–6% degrees of a garnet-peridotite source (Comin-Chiaramonti et al. 1991, 1997, 2007; Viramonte et al. 1999).

Other mafic magma types, tholeiitic basalts and K-alkaline mafic complexes and dykes are widespread in Paraguay (Comin-Chiaramonti and Gomes 1996), whereas
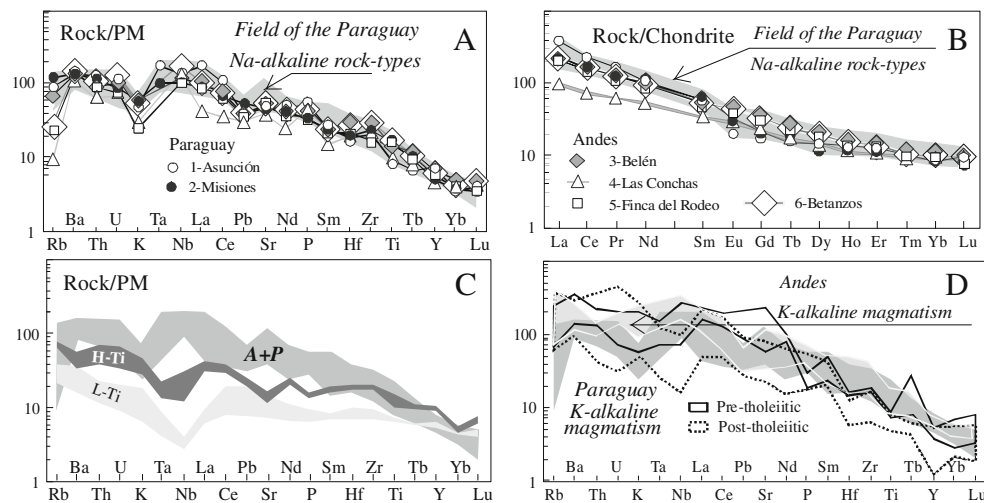
Fig. 3 a Trace elements, averaged compositions, normalized to the primitive mantle (Sun and McDonough 1989) of the mafic Na-alkaline rocks from Paraguay and Andes compared with the whole population (grey field) of the Paraguay mafic (sodic) analogues. **b** REE chondrite-normalization (Boynton 1984). Data source as in Fig. 2. **c** field of Na-alkaline magmatism (Andes + Paraguay: A + P) compared with Lower Cretaceous tholeiitic magmatism from Paraguay (H-Ti and L-Ti, high and low Ti variants, respectively). **d** the same Na-alkaline magmatism compared with the K-alkaline magmatism from Paraguay and Andes, pre-tholeiitic (>138 Ma) and post-tholeiitic (<129 Ma). Data sources: Comin-Chiaramonti et al. (2001, 2007), Lucassen et al. (2007)

K-alkaline magmatism is subordinate in Andes (Lucassen et al. 2007). Trace element pattern of high-Ti and low-Ti variants of the tholeiitic magmatism from Paraguay are different and especially the Ta and Nb contents are lower than in the Na-alkaline rocks (Fig. 3c; Comin-Chiaramonti et al. 2007). Paraguayan K-alkaline rocks show a broad range of incompatible element (I.E.) contents. The pre-tholeiitic K-alkaline rocks display positive spikes of Sm and Tb, whereas their post-tholeiitic equivalents have pronounced Nb, Hf and Y negative spikes (Fig. 3d; Comin-Chiaramonti et al. 1997). The rare Andean K-magmatism differs mainly by higher Rb-K-Nb contents from the Na-alkaline rocks of similar age (Fig. 3d).

Radiogenic isotopes

Sr-Nd-Pb isotope signatures are widely used to distinguish between mantle sources, e.g. between EMI, DMM (depleted mantle) and HIMU components (EMI = enriched mantle, low in Nd, DMM = depleted mantle, HIMU = high U/Pb, μ, component: Zindler and Hart 1986; Hofmann 1988). Substantial crustal contamination in the analyzed alkaline rocks is precluded, and Sr, Nd, and Pb isotope compositions (Table 1) represent largely the isotopic composition of the mantle source (Comin-Chiaramonti et al. 1997, 2007; Lucassen et al. 2007 and enclosed references).

Sr, Nd, and Pb initial isotope ratios of Cretaceous-Paleogene Na-alkaline rocks, Cretaceous potassic rocks, and Lower Cretaceous tholeiites (Comin-Chiaramonti and Gomes 1996, 2005) from Paraguay and Na-alkaline rocks from the Central Andes (Lucassen et al. 2002, 2007;

Schultz et al. 2004) follow similar trends plotting between HIMU and EMI end-members (Fig. 4a–c).

It is noteworthy that the isotopic compositions, particularly the $^{207}Pb/^{204}Pb$ vs. $^{87}Sr/^{86}Sr$ and $^{143}Nd/^{144}Nd$ ratios, develop towards the HIMU rather than to the DMM compositions. A HIMU component likely played an important role in the Na-alkaline magmatism. Cretaceous potassic and tholeiitic magmatism from Paraguay shows more affinities to EMI. The Cretaceous K-magmatism from Andes displays lower initial $^{86}Sr/^{87}Sr$ and higher $^{143}Nd/^{144}Nd$ than K-magmatism from Paraguay (Fig. 4). The variable isotopic composition of the intra-plate magmatism indicates mantle heterogeneity during Mesozoic times at the respective locations.

Mantle xenoliths

Variable enrichments of incompatible elements are commonly observed in contradiction to the refractory composition of the majority of the mantle xenoliths, thus requiring additional processes besides partial melting and fractionation (Roden et al. 1984 and enclosed references). Such processes have been generally called "metasomatic" (Menzies and Hawkesworth 1987) and the metasomatism of residual peridotites by volatile-charged fluids or small-volume melts carrying incompatible elements, causes different styles of enrichments. Metasomatically changed parent/daughter element ratios could develop isotopic inhomogeneities by radioactive in situ decay in a non-convective, lithospheric mantle.

Table 1 Averaged isotopic analyses, time integrated ratios (i: initial ratio; μ: $^{238}U/^{204}Pb$ and κ: $^{232}Th/^{238}U$) for sodic-alkaline magmas from Paraguay and Andes

Location	Asunción	Misiones	Belén	Las Conchas and Cadillal	Finca del Rodeo	Betanzos	Ayopaya carbonatite
N. of samples	10	6	3	2	3	6	1
Notional Age	59	118	130	100	96	82	98
Rb	56±20	87.5±11.9	42±16	5.8±2.3	14.7±2.9	16.7±5.4	<0.1
Sr	1,080±76	1,025±70	1,097±76	798±4	1,080±174	1,147±135	13,440
$(^{87}Sr/^{86}Sr)_i$	0.70367	0.70425	0.70380	0.70363	0.70418	0.70339	0.70329
±	0.00011	0.00016	0.00022	0.00004	0.00041	0.00022	0.00001
Sm	10.11±1.66	11.01±1.44	11.3±0.5	6.5±0.1	9.4±0.3	10.6±1.5	86.0
Nd	59.93±8.78	61.5±7.2	60.7±1.8	31.5±0.1	50.3±0.7	58.7±11.8	538.4
$(^{143}Nd/^{144}Nd)_i$	0.51268	0.51242	0.51267	0.51275	0.51274	0.51274	0.51273
±	0.00006	0.00001	0.00001	0.00001	0.00001	0.00001	0.00001
ε_{Sr}	−13.81	−4.46	−10.68	−13.54	−5.73	−17.15	−18.40
ε_{Nd}	2.30	−1.24	3.78	4.68	4.34	4.31	4.30
U	2.00±0.03	1.47±0.52	2.12±0.11	1.45±0.01	1.58±0.13	2.73±0.58	3.48
Th	10.50±0.63	7.11±1.93	7.88±0.003	5.32±0.45	7.78±0.12	9.56±1.60	13.15
Pb	10.06±0.26	7.31±2.52	7.26±0.62	5.55±0.04	7.06±0.31	5.47±1.59	22.16
$(^{206}Pb/^{204}Pb)_i$	18.89±0.07	18.31±0.14	19.29±0.08	18.63±0.00	19.13±0.01	19.39±0.17	19.20
$(^{207}Pb/^{204}Pb)_i$	15.67±0.01	15.68±0.00	15.57±0.01	15.56±0.00	15.58±0.01	15.59±0.01	15.64
$(^{208}Pb/^{204}Pb)_i$	38.37±0.17	37.97±0.01	39.09±0.07	38.25±0.05	39.16±0.02	39.06±0.18	39.15
μ	12.78	12.79	19.11	16.75	14.58	25.52	10.18
κ	5.42	5.00	3.84	5.64	3.79	3.62	3.90

For comparison the Apoyaya carbonatite, 100 Ma, is shown (Schultz et al. 2004 and Lucassen et al. 2007). Data source: Comin-Chiaramonti et al. (1991, 1997, 2001), Velázquez et al. (2006) and Lucassen et al. (2002, 2007)
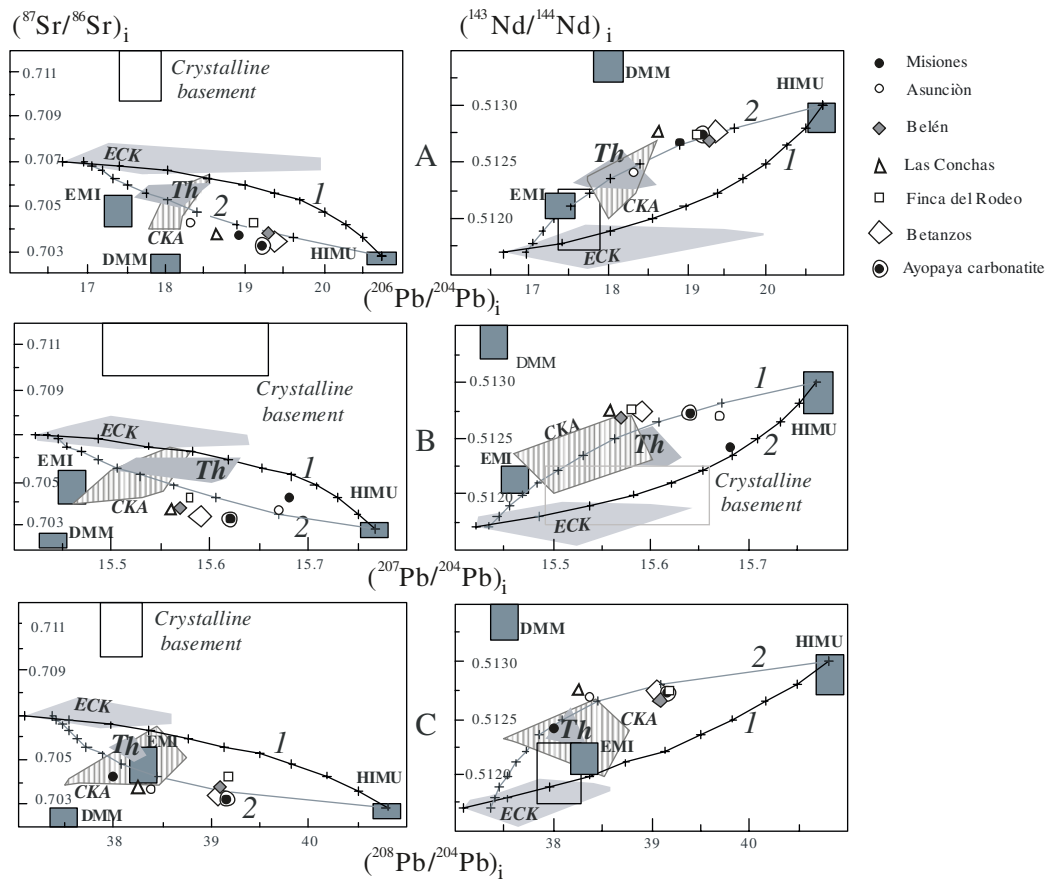
Fig. 4 Sodic lavas plot in the Sr, Nd vs Pb isotopic (time integrated) diagrams. **A**, **B**, **C**: *1* and *2*, isotopic mixing curves between HIMU and potassic magmas from Lower Cretaceous potassic rocks (ECK, Eastern Paraguay), computed using the following isotopic composition: **HIMU** (St. Helena; Chaffey et al. 1989), $^{87}Sr/^{86}Sr = 0.70282$, $Sr = 650$ ppm, $^{143}Nd/^{144}Nd = 0.5130$, $Nd = 40$ ppm, $^{206}Pb/^{204}Pb = 20.73$, $^{207}Pb/^{204}Pb = 15.77$ and $^{208}Pb/^{204}Pb = 40.80$, $U = 1.44$ ppm, $Th = 3.88$ ppm, $Pb = 4$ ppm, $\mu = 24.4$, $\kappa = 2.78$; **ECK**, *1*: $^{87}Sr/^{86}Sr = 0.7070$, $Sr = 1,300$ ppm, $^{143}Nd/^{144}Nd = 0.5117$, $Nd = 60$ ppm, $^{206}Pb/^{204}Pb = 16.672$, $^{207}Pb/^{204}Pb = 15.422$, $^{208}Pb/^{204}Pb = 37.10$, $U = 1.47$ ppm, $Th = 6.38$, $Pb = 2$ ppm, $\mu = 23.09$, $\kappa = 4.80$; **ECK**, *2*: $^{87}Sr/^{86}Sr = 0.7070$, $Sr = 1,300$ ppm, $^{143}Nd/^{144}Nd = 0.5117$, $Nd = 60$ ppm, $^{206}Pb/^{204}Pb = 16.945$, $^{207}Pb/^{204}Pb = 15.434$, $^{208}Pb/^{204}Pb = 37.369$, $U = 2.40$ ppm, $Th = 9.10$ ppm, $Pb = 15$ ppm, $\mu = 9.8$, $\kappa = 3.8$. Crosses: 10% step of mixing. Data sources: DMM, HIMU and EMI, Hart and Zindler (1989); crystalline basement as in Comin-Chiaramonti and Gomes 2005; tholeiitic (Th) and K-alkaline magmatism (ECK, CKA, Paraguay and Andes, respectively), Comin-Chiaramonti and Gomes (1996, 2005), Comin-Chiaramonti et al. (1997, 2007) and Lucassen et al. (2002, 2007); Ayopaya carbonatite (Schultz et al. 2004)

Petrology and major element composistion

Mantle xenoliths are particularly abundant in the melanephelinites-ankaratrites from Ñemby hill (Asunción, Paraguay) and in basanites from Las Conchas Valley (Andes; cf. Fig. 1). Based on the aproach of Spera (1984), Comin-Chiaramonti et al. (1991), suggest that transport of the xenoliths to the surfaced occurred in a very short time, e.g. less than 9 days (assuming a diameter of 45 cm, corresponding to the size of the largest xenoliths, a density of 3.3 g/cm³ and an origin of the hosting liquids from depth ~70–75 km, i.e. ~boundary between garnet and spinel peridotite).

The xenoliths are mainly spinel-lherzolites, harzburgites and subordinate dunites. The dominant texture is protogranular, rarely tabular or porphyroclastic (De Marchi et al. 1988; Viramonte et al. 1999; Lucassen et al. 2005). The Paraguay mantle xenoliths contain variable amounts of glassy patches ("blebs", according to Menzies et al. 1987 and Comin-Chiaramonti et al. 2001), and glassy drops in clinopyroxenes. The latters show an overprinted spongy texture, mainly characteristic of the clinopyroxenes of the high potassium suite (H-K, see below). The blebs (mg# 0.88–0.91) mainly consist of a glassy matrix containing microlites of olivine (mg# 0.91–0.92), clinopyroxene (mg# 0.91–0.93), Cr-spinel and (rarely) phlogopite (mg# 0.86–0.92). According to Comin-Chiaramonti et al. (1986, 1991, 2001) and Wang et al. (2007) they were formed by decompression melting of amphibole and phlogopite.

In the Andes, clinopyroxene of some samples shows rims of secondary pyroxene with sieve texture and pockets of devitrified glass, which were attributed to decompressional melting during rapid ascent (Lucassen et al. 2005).
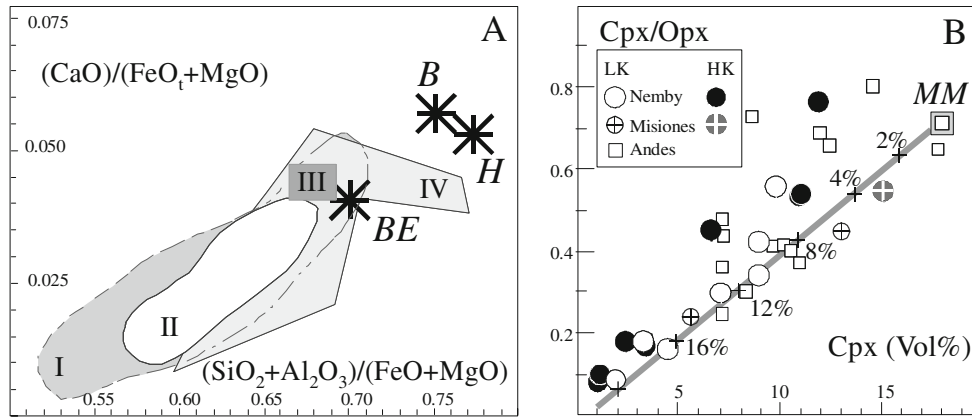
Fig. 5 a ($SiO_2 + Al_2O_3$)/($FeO_t + MgO$) vs CaO/($FeO_t + MgO$) diagram (molar ratios) for bulk-rock compositions relative to the Paraguay xenoliths, Asunción, LK (I), HK (II) and Misiones (III), respectively, and Andean suites (IV). Stars *B*, *H* and *BE*: pyrolite compositions (Bristow 1984), primitive mantle (Hofmann 1988) and Bulk Earth (McKenzie and O'Nions 1991), respectively. **b** variation of the modal cpx vs the modal cpx/opx ratio. The line indicates model variation trends induced by non-modal fractionation melting in a primitive mantle composition (Rivalenti et al. 2000); thicks are at 4% melting intervals; *MM*, mantle mode after Rivalenti et al. 1996. Data sources: De Marchi et al. (1988) and Lucassen et al. (2005)

The rapid ascent is also testified by the lack of any apparent interactions between the mantle xenoliths and host lavas (De Marchi et al. 1988) and by lack of phase transitions in the associated crustal xenoliths (e.g. plagioclase-microcline, quartz-sillimanite pairs for which the calculated T-P equilibria are between 570° and 700°C and between 0.40 and 0.85 GPa, respectively; Comin-Chiaramonti et al. 2001).

The Paraguayan xenoliths are characterized by a large range of K_2O contents (0.02 to 0.51 wt %). Some xenoliths have K_2O abundances comparable or even higher than those reported for metasomatized mantle peridotites (e.g.

Roden et al. 1984), resembling in some case to amphibole-mica-apatite bearing mantle-xenolith suites (O'Reilly and Griffin 1988). K_2O contents and the abundance of blebs and glassy drops allow to group the Paraguay xenoliths into two main suites, i.e. a low-K suite (LK, $K_2O < 0.1$ wt %, and relatively low in incompatible elements), and a high-K suite, the latter with abundant glassy drops and/or variable amounts of blebs and spongy clinopyroxenes (HK, $K_2O \geq 0.2$ wt % and with high contents of incompatible elements). On the other hand, the Andean xenoliths have K_2O content < 0.08 wt% (average 0.03 ± 0.02 wt%). Some nodules show important modal carbonates (carbonatized xenoliths of

Fig. 6 a, **b** Al_2O_3 vs CaO and Cr_2O_3 (wt%) for orthopyroxenes from spinel xenoliths. Spinel peridotite field is from Gregoire et al. (2005) and enclosed references. **c** mg# [molar MgO/ (MgO + FeOt)] vs Na_2O (wt%). Data sources as in Figs. 3 and 4
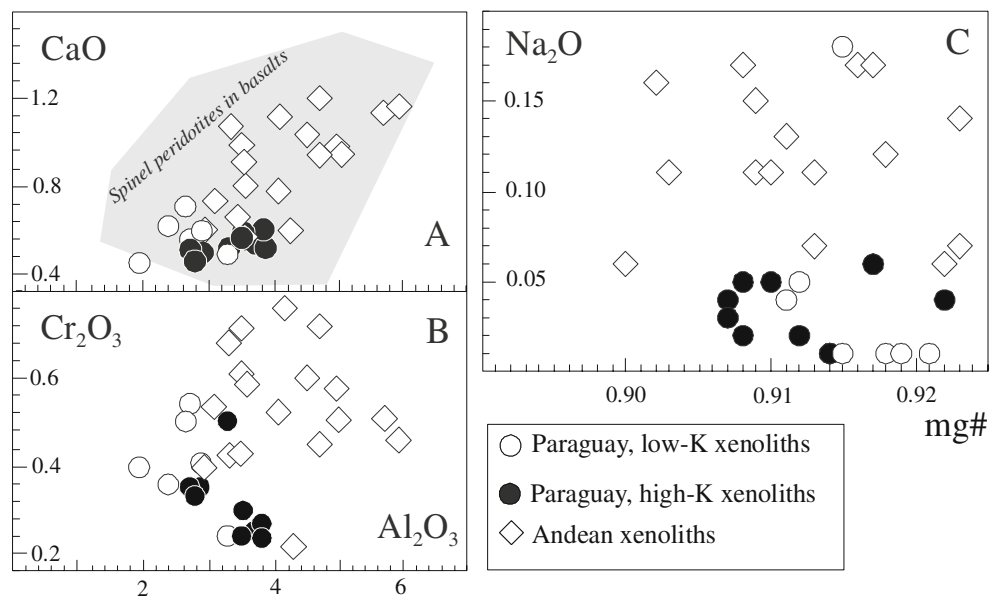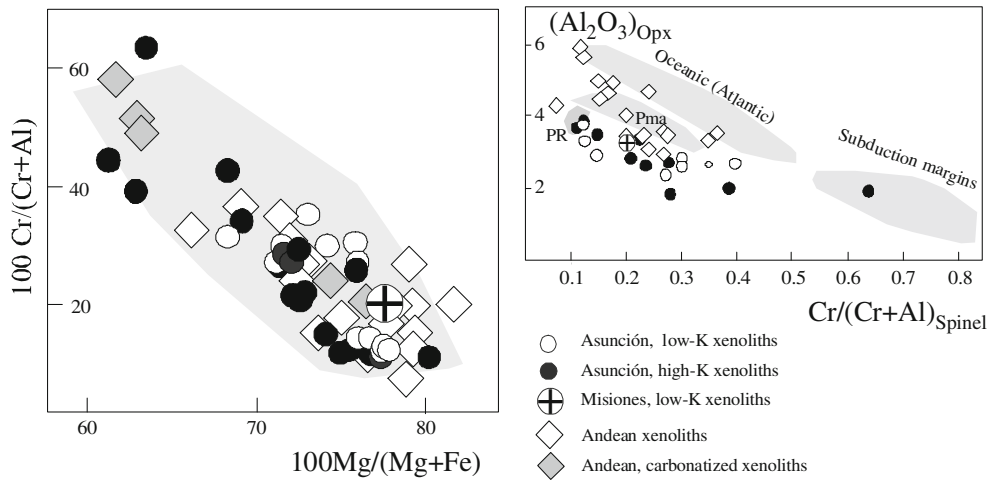
Fig. 7 Mg-number (atomic 100 Mg/(Mg + Fe) vs. Cr-number [100 Cr/(Cr + Al)] for spinel from spinel peridotites of Paraguay and Andes. Dark grey diamonds: Andean carbonatized xenoliths; large crossed circle: LK xenolith from Misiones Province (Paraguay). Other symbols and field as in Fig. 6. Data source as in Figs. 3 and 4. **Inset**: Cr/(Cr + Al) (spinel) vs. Al_2O_3 (orthopyroxene) for the studied xenoliths. Fields for mantle peridotites (Bonatti and Michael 1989) are also shown; Pma, passive margins; PR, preoceanic rift

Lucassen et al. 2005). Complete sets of chemical analyses are in De Marchi et al. (1988) and Lucassen et al. (2005).

Coherent variations of major element contents in both suites follow a lherzolite-dunite sequence between primitive and very depleted mantle composition (Fig. 5a). The population is mainly represented by lherzolitic-harzburgitic (dunitic) compositions, most samples ranging between a molar $(SiO_2+Al_2O_3)/(MgO+FeOt)$ ratio of 0.55–0.63 . The residual character of the harzburgitic mantle xenoliths is consistent with melting of lherzolite and basalt-component removal, which is also evidenced by the decrease in the cpx/opx modal ratio with decreasing modal cpx (Fig. 5b; Rivalenti et al. 1996 and Comin-Chiaramonti et al. 2001).

Mineral composition

Chemical analyses and methods are available in the following previous papers: Comin-Chiaramonti et al. (1986, 1991, 2001), Comin-Chiaramonti and Gomes (1996), De Marchi et al. (1988) and Lucassen et al. (2005). Here, the main characteristics of the minerals from various suites and domains are summarized.

Olivine The olivines are quite homogeneous in composition within each sample, and their forsterite component ranges from 89.5 (lherzolites) to 93 mole% (dunites). The NiO_2 and CaO contents range between 0.28–0.41 and 0.02–0.12 wt%,

Fig. 8 Mg-number (atomic 100 Mg/(Mg + Fe) vs. SiO_2, Al_2O_3, Cr_2O_3, Na_2O (wt%) and Al^{VI}/Al^{IV} (a.f.u.) in analyzed clinopyroxenes from Paraguay and Andes. Inset: Clinopyroxene fields in the pyroxene quadrilateral; I and II LK and HK from Asunción and III from Misiones (LK and HK); IV, Andes. Data source: Comin-Chiaramonti et al. (1991), Comin-Chiaramonti and Gomes (1996; 2005), Lucassen et al. (2005). Al^{VI}/Al^{IV} of Paraguayan samples after Princivalle et al. (2000); the structural data for Andean clinopyroxenes were calculated from microprobe analyses following the method described in Nimis (1995) and enclosed references
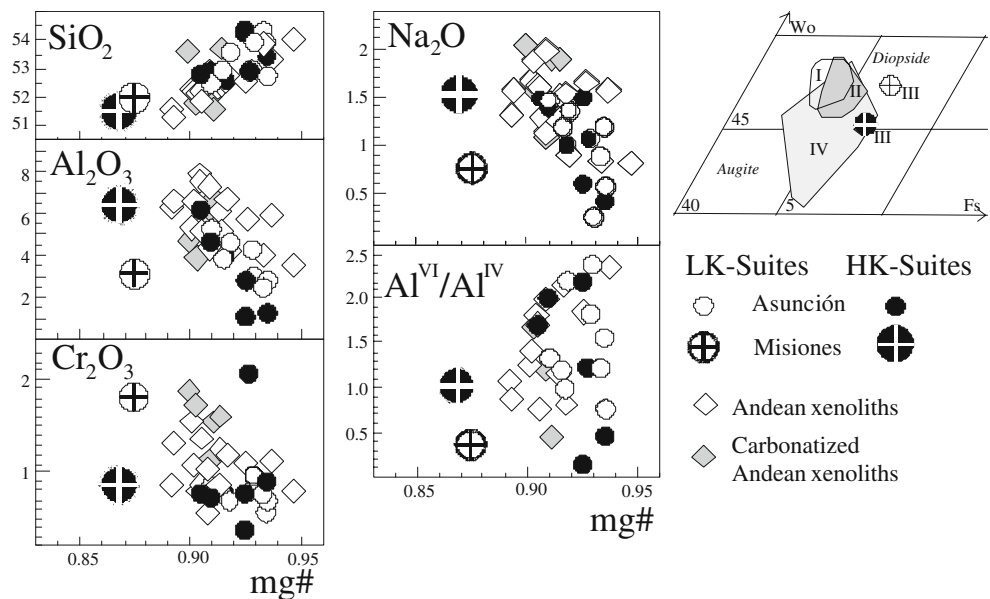
respectively and are not correlated with the forsterite contents in both Andean and Paraguayan samples (averages: NiO_2 wt%, 0.34 ± 0.01, Paraguay, and 0.34 ± 0.04, Andes; CaO wt%, 0.05 ± 0.03, Paraguay, and 0.08 ± 0.02, Andes).

Orthopyroxene Orthopyroxenes (Opx) are commonly unzoned and rarely show spinel exsolutions. They are enstatites with mg# [molar $MgO/(MgO+FeOt)$] varying from 0.91 to 0.92 in Paraguayan xenoliths (both LK and HK suites), and from 0.90 to 0.93 in Andean nodules. Most of the Opx compositions plot in the field of the "spinel peridotites in basalts" (Fig. 6a). Many Andean Opx are distinguished from their Paraguayan analogues by higher contents of Al_2O_3, CaO, Na_2O and Cr_2O_3 (Fig. 6a–c). On the other hand, Na_2O shows a very large range of the concentrations (LK suite from Paraguay from 0.01 to 0.18 wt% for the same mg# = 0.916; Fig. 6c).

Spinel Spinels are magnesian-aluminous chromites that mainly plot inside the field of the "spinel peridotites in basalts" (Fig. 7; Fig. 4 of Gregoire et al. 2005). Mg- and Cr-number range from 61 to 82 and from 8 to 64, respectively. Spinels from xenoliths with $K_2O\geq0.20$ wt % (see below) are generally characterized by Cr increase from the core to the rim, particularly of grains inside the blebs, while spinels from xenoliths with $K_2O<0.1$ wt % are unzoned (De Marchi et al. 1988).

The composition of the xenoliths encompasses (inset of Fig. 7) the various oceanic settings reported by Bonatti and Michael (1989) and tend to fit the field of the passive margins. In particular, it should be noted that the spinels rom carbonate-bearing xenoliths show the higher Cr/(Cr + Al) ratios. Moreover some Paraguay samples (both HK and LK suites) plot in the field of preoceanic rift, and only one sample (Asunción rift, HK!) plot in the field of subduction-related margins (Fig. 7).

Clinopyroxene Clinopyroxenes (Cpx), according to the classification of Morimoto (1989), have "quadrilateral" components >87%, and are diopside in the Paraguay xenoliths, showing a very narrow compositional range (Wo 46.2–48.4, En 47.8–49.7, Fs 3.4–5.1), but in the Andes they vary from augite to diopside (Wo 40.1–47.9, En 45.0–53.8, Fs 3.0–6.2; s. inset of Fig. 8). There is a

compositional overlap between Paraguayan and Andean Cpx in variable mg# (0.86 to 0.94) versus major element contents and Al^{VI}/Al^{IV} (Fig. 8).

Commonly, Cpx also show lamellar spinel (rarely lamellar orthopyroxene) exsolutions cut by the glassy drops. The integrated compositions of the spongy Cpx (obtained by shifting the sample under defocussed beam in order to provide an estimate of composition before unmixing) are particularly rich in K_2O (up to 1.22 wt %) and in Al_2O_3, Rb, Sr, and Ba (De Marchi et al. 1988), reflecting the occurrence of the glassy drops (up to ~7.5 wt% of the cpx, as from mass balance).

Sulfides The available data are exclusively from the Asunción Province, although sulfide inclusions are reported by Lucassen et al. (2005) also in Andean xenoliths. Sulfides are pyrrhotite and pentlandite of small size (< 8 μm) and inhomogeneously distributed (Comin-Chiaramonti et al. 1986). Nevertheless, the bulk S content displays a negative correlation ($r=-0.95$) with the mg#$_{Opx}$ (Fig. 9), suggesting some relationships between sulfur abundances and the "residuality" of the xenoliths. On the other hand, S-K_2O correlation does not exist (Fig. 8). S is generally believed to be metasomatic in origin or derived from immiscibile sulfide melt (MacRae 1979). If a metasomatic event was responsible for the S contents, it must have added S prior to melting of the mantle xenoliths.

Carbonate In Paraguay carbonate (mainly Mg-calcite) is present in pockets in the glassy patches, or as carbonate veins along the grain boundaries ($MgCO_3$ about 5–10 wt% and<0.6 wt%, respectively). Measured $\delta^{18}O‰$ (V-SMOW) and $\delta^{13}C‰$ (PDB) in some samples (Comin-Chiaramonti et al. 1991) are in the ranges $+8.5\div+18.9$ and $-5.2\div-7.92$, respectively (Fig. 10), i.e. values that plot spanning the field believed typical of primary carbonatites (Keller and Hoefs 1995) to the field of the O-C fractionated carbonates from the Juquiá carbonatite (Comin-Chiaramonti and Gomes 2005). In the Andes occurrences, Lucassen et al. (2005) report the presence of carbonatized peridotites, similar in shape and size to the other peridotite xenoliths. Minor clinopyroxene and spinel and occasional phogopite are set in a matrix of carbonate grains. $\delta^{18}O‰$ and $\delta^{13}C‰$ range from +17.3 to +20.7 and from −5.3 to −8.9, respectively,

Fig. 9 Bulk S abundances (ppm) in Paraguay xenoliths vs mg#$_{Opx}$ and vs bulk K_2O. Data source: Comin-Chiaramonti et al. (1986)
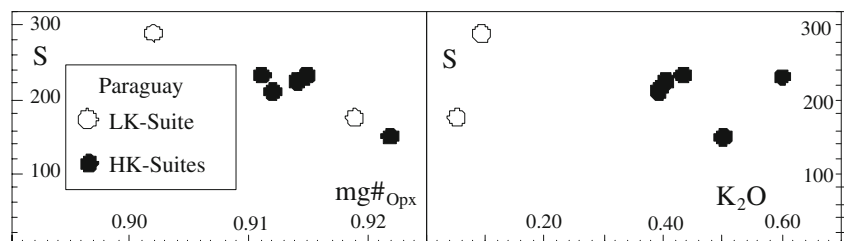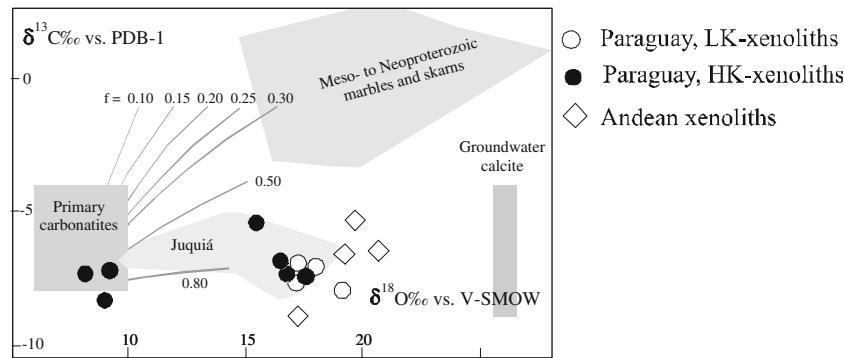
Fig. 10 $\delta^{18}O‰$ (V-SMOW) vs. $\delta^{13}C‰$ (PDB-1) for carbonates from mantle xenoliths. Symbols as in Fig. 8. The line labelled f, correspond to the model elaborated by Speziale et al. (1997), where $f=[(A-b)/A]$, $A = CO_2$ initial molar concentration and b = molar concentration in the fluid-mineral system at the time "t". Fields: Primary carbonatite after Keller and Hoefs (1995), Meso- and Neoproterozoic marbles and skarns, groundwater calcite and Juquiá carbonatite after Comin-Chiaramonti and Gomes (2005), and enclosed references

($^{87}Sr/^{86}Sr$: 0.7078 to 0.7014), pointing to post-magmatic and/or deuteric groundwater processes in the carbonate formation (Comin-Chiaramonti and Gomes 2005 and enclosed references).

Blebs Incompatible element ratios of xenoliths and blebs are very different from those of their host lavas. This precludes an origin of the high abundances of incompatible elements in the xenoliths and blebs from contamination by host lavas. Some bulk compositions, along with K/Ba, K/Rb and Ba/Sr average ratios of the blebs, mantle xenoliths and host lavas are listed in Table 2.

The compositional similarity, and in particular the high contents of Na_2O and K_2O, between the Paraguay blebs and mantle-derived hydrous phases (Shaw and Klügel 2002 and enclosed references), suggests that amphibole and phlogopite were present in the Paraguay xenoliths at some time. Mass balance calculations show amphibole + phlogopite contents ranging from 4.8 to 9.0 wt% and the amphibole/phlogopite ratio varying from 0.8 to 1.1 wt% (average 0.92 ± 0.17; Table 5 of Comin-Chiaramonti et al. 1986).

The absence of hydrous phases in Paraguay mantle xenoliths does not invalidate this hypothesis: if the xenoliths were sampled at a relatively high temperature, the abrupt decrease of P-load, due to the rapid magma rise, could have produced the complete melting of any hydrous phase.

Also some xenoliths from Andes (LK) show glassy pockets and amphibole associated with the equilibrium mineral assemblage (Lucassen et al. 2005). Pargasite (sample A-104 of Table 2) show a composition very similar to those of amphiboles believed to be mantle phases (Shaw and Klügel 2002 and enclosed references).

Thermobarometry

In Paraguay, equilibration temperatures for orthopyroxene-clinopyroxene pairs (Wells 1977) and for olivine-spinel pairs (Fabriès 1979) vary between 862 and 1,075°C and between 748 and 968°C, respectively (De Marchi et al. 1988). In Andes xenoliths, the Wells geothermometer gives roughly equivalent temperature, ranging from 900 to 1,100°C (Lucassen et al. 2005). Intracrystalline temperatures (calculated for all the samples according to Mercier 1980, Mercier et al. 1984; cf. Sen et al. 1993 for a detailed discussion) for clinopyroxene and orthopyroxene pairs, vary as average between 936 and 1,033°C (Paraguay, LK-suite), 920 and 1,120°C (Paraguay, HK-suite), 936 and 1,160°C (Andes). The pressures are roughly in the range 1.1–2.3 GPa in all the suites (Table 3), where the higher pressures where obtained for the more depleted xenoliths of the LK-suites.

The oxygen isotope compositions on separates of clinopyroxene and coexisting olivine ($\delta^{18}O‰$) range from 5.5 to 6.0‰, and from 5.0 to 6.1‰, respectively, both in Paraguay and in Andes (Table 3). These measured isotopic ratios are in the range of values for worldwide mantle phases (olivine 4.4 to 7.5‰, clinopyroxene 4.8 to 6.7‰: Chiba et al. 1989) and for South America mantle xenoliths (olivine 4.9 to 6.4‰, clinopyroxene 5.0 to 6.0‰; Kyser 1990). The calculated Cpx-Ol isotopic temperatures (according to Kyser et al. 1981) are around 970–1,070°C and 1,030–1,130°C (LK suite, Paraguay and Andes) and 1,100–1,180°C (HK suite, Paraguay), suggesting equilibration temperatures higher in the HK suite than in LK suite. However, it can be observed that the highest temperature of the HK suite is substantially due to higher $\delta^{18}O‰$ in olivine than $\delta^{18}O‰$ in clinopyroxene: according to Perkins et al. (2006), the relatively low $\delta^{18}O$ in the pyroxenes reflects metasomatism by a silicate melt from subducted altered oceanic crust. Therefore the Paraguayan HK suite should be the best candidate to a subduction-linked environment.

According to Princivalle et al. (2000), the investigated Paraguay clinopyroxenes have V(Cell) and V(M1) sites intermediate between those of plagioclase- and garnet-

Table 2 Representative chemical analyses of blebs (glassy patches: 3198 and 3211, H-K lherzolite and harzburgite, respectively), average of blebs bearing xenoliths and blebs free xenoliths from Paraguay, and represen-tative chemical analyses of glassy pocket-bearing Andean xenoliths (with diopsidic clinopyroxene: **, and augitic clinopyroxene: ***) along with coexisting amphibole

	Bleb (3198)	Bleb (3211)	HK-Suite (Paraguay) $N=8$	LK-Suite (Paraguay) $N=25$	LK-Andes** A-98d	LK-Andes*** A-102	LK-Andes*** A-104	Amph A-104
wt%								
SiO_2	44.21	42.61	43.42±1.11	43.32±2.78	42.1	43.5	45.4	43.84
TiO_2	0.45	0.66	0.06±0.04	0.02±0.01	0.17	0.02	0.17	1.64
Al_2O_3	7.83	9.29	1.78±0.43	1.18±0.47	1.5	2.2	3.9	15.14
Cr_2O_3	4.00	4.28	0.76±0.14	0.78±0.15	0.81	0.81	0.75	0.76
FeO_{tot}	6.51	6.35	8.16±0.36	7.78±0.26	8.1	7.6	8.0	3.90
MnO	0,12	0.17	0.14±0.01	0.12±0.02	0.1	0.1	0.1	0.03
MgO	28.57	22.54	43.19±1.97	44.92±1.58	43.6	40.7	37.1	16.75
CaO	4.18	5.99	1.55±0.82	1.18±0.54	2.6	2.7	3.8	10.34
Na_2O	1.30	2.35	0.27±0.09	0.09±0.04	0.17	0.23	0.37	3.62
K_2O	1.90	2.93	0.44±0.08	0.07±0.03	0.08	0.03	0.03	0.31
P_2O_5	0.59	0.85	0.09±0.08	0.01±0.01	0.02	0.03	–	–
Sum	99.66	98.02	99.86	99.47	99.25	97.81	99.65	96.53
ppm								
Ba	295	823	43.8±11.9	5.6±3.4	5.5	3.5	4.9	
Rb	33	87	8.7±3.5	2.9±1.4	2.1	2.4	2.5	
Sr	625	990	75±51	14.6±5.9	17.9	22.2.	14.3	
K/Ba	53.4	29.6	83.4	103.8	120.8	71.2	50.8	
K/Rb	478	280	420	200.4	316.3	103.8	99.6	
Ba/Sr	0.47	0.83	0.58	0.38	0.31	0.16	0.34	
Mantle Phases**								
ol			71.26±6.89	72.4				
opx			16.79±4.74	22.5				
cpx			4.48±2.91	3.9				
sp			1.23±0.28	1.2				
amph			2.97±2.97					
phlog			3.27±0.80					
Σr^2			0.51±0.37					
amph/phlog			0.92±0.16					

Mantle phase abundances calculated by a least square program, using amphibole and phlogopite compositions from Comin-Chiaramonti et al. (1986, 1991) and enclosed references. Other data source: Comin-Chiaramonti et al. (2001), De Marchi et al. (1988), Lucassen et al. (2005)

bearing mantle peridotites, i.e., in a pressure range between 1.2 and 2.2 GPa. Thus, also the isotopic and crystallographic results fit the inter and intracrystalline thermobarometry (note also the correlation between Kyser isotopic temper-atures and Mercier temperatures in the inset of Fig. 11).

The Paraguayan and Andean xenoliths define an apparent common geotherm (Fig. 11) that, starting at about 830°C and 1.0 GPa at the transition mantle-crust (see also Fig. 16 of Lucassen et al. 2005), intersects the hydrous peridotite solidus at about 1,140°C and 2.1–2.2 GPa in the spinel-peridotite facies, near to the transition with the garnet-peridotite facies, which is believed to be the source of the sodic alkaline magmatism (Comin-Chiaramonti et al.

1991, 2001; Princivalle et al. 2000). Moreover, a lot of samples plot along the solidus representing a peridotite with $CO_2/(CO_2 + H_2O) = 0.8$ of Moore et al. (2008).

Clinopyroxenes: trace elements and radiogenic isotopes

Clinopyroxenes (Cpx) from mantle xenoliths are the main carrier for many trace elements (e.g., Sr, U, Th, Pb, and REE in garnet and amphibole free paragenesis; Gregoire et al. 2005 and enclosed references), and have a considerable importance to understand the mantle processes, such as melting, metasomatism and sub-solidus re-equilibration

Table 3 Temperature (°C) and pressure (GPa) estimates for the peridotite xenoliths calculated as averaged values of intracrystalline temperatures of clinopyroxene and orthopyroxene (in parenthesis the standard deviation) following thermobarometry (1) of Mercier (1980); (2) isotopic values, expressed as δO^{18} ‰ notation, and extimated temperatures of isotopic equilibration, following Kyser (1990)

Sample no.	T (°C)	P (GPa)	δO‰^{18} Cpx	δO‰^{18} Ol	T(°C)	Sample no.	T (°C)	P (GPa)	δO‰^{18} Cpx	δO‰^{18} Ol	T(°C)
Paraguay						Andes					
LK						LK					
3091	950(45)	1.28(0.18)				A-94	1,020(14)	2.02(0.11)			
3192	975(20)	1.72(0.10)	5.8	5.0	969	A-98d	1,159(97)	2.12(0.11)	5.8	5.5	1,093
3199	990(15)	1.98(0.09)				A-101	1,052(46)	2.06(0.11)			
3221	1,028(30)	2.04(0.15)	5.9	5.2	997	A-102	1,126(37)	2.28(0.08)			
3227	979(55)	1.70(0.20)	5.8	5.3	1,048	A-104			5.6	5.3	1,101
3252	1,003(25)	1.87(0.14)				A-106	1,028(11)	1.99(0.01)			
3254	936(18)	1.29(0.13)				4-147	936(10)	1.69(0.02			
3260	841(10)	1.13(0.20)				4-147k	995(23)	1.76(0.13)			
3269	1,033(41)	2.12(0.22)	6.0	5.6	1,071	4-147m	1,053(32)	1.97(0.06)	5.8	5.3	1,030
3303	1,014(35)	1.96(0.10)				00-179	1,070(14)	2.04(0.08)			
M569X	997(20)	1.40(0.20)				7-168b	1,109(27)	2.16(0.03)			
						6-178b	1,087(23)	2.06(0.10)			
HK						6-179	1,147(24)	2.15(0.23)			
						6-180	1,148(25)	2.27(0.06)	5.6	5.5	1,127
3198	988(11)	1.84(0.12)				6-181	1,077(37)	1.92(0.21)			
3211	1,104(67)	1.98(0.10)	5.6	5.8	1,183	7-169	1,115(21)	2.19(0.04)	5.7	5.4	1,087
3222	978(22)	1.78(0.18)				00-175	1,067(25)	2.08(0.03)			
3259	995(10)	1.91(0.11)				00-177	1,119(25)	2.13(0.13)			
3270	971(18)	1.85(0.12)									
3281	1,000(12)	1.96(0.08)									
3283	1,128(32)	2.10(0.28)				Carbonatized					
3284	1,005(15)	1.92(0.07)	6.0	6.1	1,169	Peridotite					
3288	983(30)	1.83(0.05)									
3293	963(25)	1.66(0.31)				A-57	1,160(10)	2.20(0.20)			
3301	881(28)	1.57(0.32)				A-113e	1,055(25)	1.70(0.10)			
3307	–		5.9	6.0	1,169	4-301	1,030(18)	1.44(0.08)			
3331	1,067(64)	2.08(0.29)	5.5	5.3	1,113	4-229	1,000(32)	1.49(0.05)			
M569	1,000(30)	1.84(0.10)									

Data source: Comin-Chiaramonti et al. (1986, 1991, 2001), De Marchi et al. (1988), Petrini et al. (1994), Lucassen et al. (2005) and F. Lucassen and B. Putlitz, unpublished data. Note the Mercier's temperature-pressure are very similar to the results obtained by means of other geothermometers and geobarometers, e.g. Nimis (1995), Brey et al. (1990) and Table 1 of Lucassen et al. (2005)

(e.g. Salters and Shimizu 1988; Laurora et al. 2001; Wang et al. 2007). The decrease of modal Cpx and depletion indexes of whole rock and Cpx (cf. Fig. 5), from fertile peridotite (primitive mantle) towards harzburgite-dunite is consistent with the extraction of melt. Melt extraction has a substantial impact on the concentrations of trace elements in the Cpx, particularly the incompatible trace elements (e.g. Rivalenti et al. 1996). In this section, we examine the relation between trace element composition and their radiogenic isotopes (Sr, Nd, Pb) of the clinopyroxenes from selected Paraguay and Andes mantle xenoliths, LK and HK suites, respectively.

Trace elements

Table 4 summarizes the ranges of trace element analyses. The main compositional characteristics can be summarized as follows (Comin-Chiaramonti et al. 2001; Lucassen et al. 2005):

(I) In the normalized trace element diagrams (Fig. 5 of Comin-Chiaramonti et al. 2001), the Paraguayan samples have patterns depleted in Ba, Nb, Zr and Ti. Furthermore, Zr and Ti display systematically negative spikes (cf. Rampone et al. 1991 for a general dis-

cussion), indicating HFSE depletion (cf. also $Zr/Zr*$ and $Ti/Ti*$ of Table 4). Sr shows both positive and negative anomalies both in LK and HK suites ($Sr/Sr*=$ 2.34 to 0.51), with the minimum in some HK harzburgite (e.g. Paraguayan 3,284 sample with $Sr/Sr*=0.51$). Sr from the Andean Cpx (LK suite) display a positive correlation with $(La/Yb)N$, [i.e. $Sr=10.76*(La/Yb)N+33,48$ with $r=0.94$; Lucassen et al. 2005].

(II) $Y/Y*$ ratio generally is near the unity (av. 0.94 ± 0.26). Notably, some xenoliths (e.g. Andean A-104 of Table 4) has a modal composition cpx 17.7, opx 27.3, ol 53.0, sp 2.0%, very similar to that of the primitive mantle (Hofmann 1988: cpx 18, opx 25, ol 55, sp 2%), and the I.E. and REE contents of the clinopyroxene display trends overlapping with those of the PMCE (Primitive Mantle Clinopyroxene Estimate; Rivalenti et al. 1996 and enclosed references). Cpx from carbonatized xenoliths display a large range of the normalized element contents between 0.1 to 10 times primitive mantle (Table 4) and variable REE patterns (Fig. 12 and Lucassen et al. 2005).

(III) LREE are commonly strongly enriched [Paraguay, La_N/Yb_N, LK suite: lherzolite = 11.9–5.4, harzburgite ~55; HK suite: lherzolite = 20.3–16.2, harzburgite = 98.2–7.9, excluding samples 3,227 (LK harzburgite with $La_N/Yb_N=0.92$) and 3,222 A,B (HK lherzolite with La_N/Yb_N from 17.66 to 0.65); Andes, La_N/Yb_N , LK: 110–0.5; Table 4 and Comin-Chiaramonti et al. 2001, Lucassen et al. 2005].

(IV) Some harzburgites both from Paraguay and Andes display U-shaped patterns, with La_N/Sm_N ~60 and

Gd_N/Yb_N ~0.55 (Tables 4 and 2 of Comin-Chiaramonti et al. 2001). Such characteristics were attributed to a "carbonatitic component" by Hauri (1997), consistent with the occurrence of carbonate phases, glassy patches and sieve clinopyroxenes.

Analyses of exsolved pyroxenes, glassy drops and patches from Paraguayan Cpx yielded the following results:

(V) Cpx from both LK and HK suites show variable enrichment of La, Ce, Sr, and Nd, from flat to fairly steep distribution patterns independently of the Cpx content, (i.e. melting degree of the xenoliths) and of the calculated temperatures. The orthopyroxene (opx) exsolutions (e.g. LK-3,254 specimen) and their host clinopyroxene have similar distribution patterns for the more compatible elements. On the other hand, K, LREE and Sr are strongly depleted in opx (Fig. 13a).

(VI) Compared with the host Cpx, the glassy drops (e.g. HK 3284 Cpx; Fig. 13b and Table 4) and patches are strongly enriched in Rb, Ba, and K, and display positive spikes for Sr ($Sr/Sr*=1.68$) and Zr ($Zr/Zr*=1.13$). Notably, the geochemical features of the glassy drops fit those of a melt from a phlogopite rich source (McKenzie and O'Nions 1991: Ti=4,796 ppm and K=78,786 ppm). The glassy patches differ from the glassy drops by their $Zr/Zr*$ (0.47 vs 1.13), $Ti/Ti*$ (0.16 vs 0.69), $Eu/Eu*$ (0.83 vs 1.14), and by a positive Nb spike. The general element distribution pattern of the glassy patches is similar to that of glasses, which were interpreted by Laurora et al.

Fig. 11 Interpretation of the P-T estimates of Table 3; symbols as in Fig. 8 (cf. Fig. 16 of Lucassen et al. 2005); (g) inferred geotherm (Petrini et al. 1994). (1) and (2) mantle crust boundary, according to Lucassen et al. (2005) and to Gibson et al. (2006). Steady-state geotherm, after Gibson et al. 2006; hydrous peridotite solidus after Hirschmann (2000); peridotite with $CO_2/(CO_2 + H_2O) = 0.8$, after Moore et al. (2008). **Inset**: relationships between Mercier (M) averaged Cpx-Opx temperatures vs Kyser (Ky) isotopic temperatures, showing the regression line ($r=0.71$)
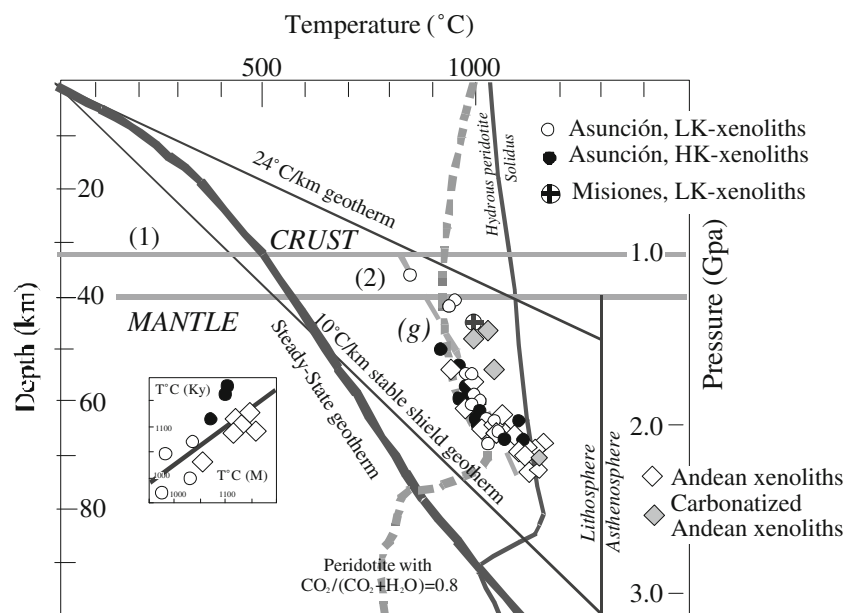
Table 4 Trace elements in clinopyroxenes (Max and min, maximum and minimum concentrations grouped as function of the Cpx content) from Paraguay (P-) and Andes (A-) mantle xenoliths, LK and HK suites, respectively, for glassy drops (GD) in clinopyroxenes and blebs in xenoliths. Elements are ordered according to their compatibility

Suite	LK		A-94	P-3221	LK		P-3252; P-3254		LK	A-4-147; A-00177; A-6-178b		LK	
Cpx%	2-3%				7-8%				8-10%			10-12%	
Samples PM	P-3269; P-3227; P-M558B				A-101; A-106; A-00179; A-6-18				P-3254			A-98d; A-6-179; A-7-169A; A-00175	
ppm	Max	Min			Max	Min	Max	Min	Opx	Max	Min	Max	Min
Rb	1.70	0.74	0.53	1.20	1.09	0.32	0.08	0.01	0.01			0.48	0.44
Ba	0.90	0.51	1.97	0.60	28.6	7.3	0.59	0.85	0.39	3.79	2.06	5.46	1.38
Nb	0.18	0.10	2.06	0.10	12.7	0.88	0.11	0.10	0.09	1.49	0.88	3.05	1.49
K	12.50	8.50		118			142	90	11.4				
La	33.32	0.41	4.58	23.70	66.1	1.89	22.84	10.87	0.32	18.7	5.55	29.9	1.01
Ce	47.48	2.18	9.63	23.64	58.2	4.1	20.98	8.72	0.07	19	8.65	46.3	2.51
Sr	234	38	97.6	425	295	7.79	132	106	1.70	172	93.5	245	29.4
Nd	9.30	2.21	5.98	3.36	10.9	1.73	3.85	0.88	0.18	10.2	4.78	22.3	2.15
Zr	11.50	5.07	16	0.80	52	7.3	0.53	0.13	0.16	35.9	17	112	18.4
Sm	0.92	0.31	1.64	0.85	1.66	0.37	0.80	0.14	0.09	2.33	1.10	5.07	0.83
Eu	0.28	0.12	0.51	0.29	0.62	0.081	0.27	0.05	0.06	0.79	0.45	1.59	0.32
Ti	420	160		1,065			750	260	314				
Gd	0.95	0.10	1.71	1.29	2.43	0.55	1.08	0.37	0.36	2.43	1.31	4.64	1.21
Dy	0.57	0.22	1.29	1.67	2.79	0.56	1.75	0.75	0.85	2.15	1.46	2.06	1.46
Y	11	3.20	5.9	2.30	15.1	3.27	12.0	6.20	7.50	10.8	6.68	13.4	6.83
Er	0.38	0.25	0.64	1.15	1.76	0.397	1.24	0.73	0.71	1.13	0.85	1.64	0.721
Yb	0.41	0.30	0.54	0.96	1.44	0.41	1.26	0.73	0.93	1.06	0.69	1.4	0.69
Sr/Sr^*	16.81	1.14	0.94	2.55	0.68	0.21	0.85	1.81	0.94	0.90	1.05	0.55	0.93
Zr/Zr^*	0.23	0.39	0.35	0.03	0.79	0.62	0.02	0.02	0.06	0.61	0.51	0.72	0.89
Ti/Ti^*	0.20	0.27		0.42			0.34	0.46	0.50				
Y/Y^*	3.09	1.71	0.84	0.22	0.89	0.91	1.07	1.07	1.25	0.90	0.78	0.95	0.86
CH													
$(La/Sm)_N$	22.78	1.03	1.76	17.53	25.05	3.21	17.96	48.83	2.24	5.05	3.17	3.71	0.77
$(Sm/Dy)_N$	2.67	2.33	5.86	0.84	0.98	5.57	0.75	0.31	0.17	1.79	1.24	4.06	0.94
$(Gd/Yb)_N$	1.87	0.27	2.56	1.08	1.36	1.08	0.69	0.41	0.31	1.85	1.53	2.67	1.42
$(La/Yb)_N$	54.79	0.92	5.72	16.64	27.25	3.11	12.17	10.04	0.23	11.89	5.42	14.40	0.99
$(Eu/Eu)^*$	0.91	1.65	0.92	0.85	0.94	0.62	0.89	0.63	0.89	1.01	1.14	0.98	0.97
Suite	LK		LK	LK	LK	HK	HK	HK	HK	HK	HK	HK	HK
Cpx%	12-15%		17.7%	Carbonatized peridotite	1%		3.4%		6.6%	10-12%		GD	Bleb

Samples	PM	A-7-168b		A-104	A-57; A-113-c; A-4-229; A-4-301a		P-328; P-SI-2A		P-3211	P-3307	P-3311; P-3222		P-3284	P-3211
ppm		Max	Min		Max	Min	Max	Min	Min		Max	Min		
Rb		0.24	0.20	0.28	2.65	0.45	1.40	1.10	1.80	0.30	1.30	0.07	120	87
Ba		3.41	2.53	1.03	37.5	1.93	4.47	2.10	3.50	0.25	0.60	0.50	1,781	823
Nb		8.6	6.4			0.49	0.30	0.25	0.70	0.30	0.20	0.11	155	277
K							3.81	81	397	10	90	30	82,453	20,091
La		28.12	7.09	1.36	10.7	0.36	38	323	119.4	23	36.14	0.58	77.39	29
Ce		20.6	19.9	3.95	25.5	1.16	98	68.4	121.5	22	45.55	0.38	106.25	68
Sr		119	110	70.1	268	132	525	248	977	130	336	18.4	1,414	990
Nd		11.5	11	3.62	25.3	1.04	62	8.89	15.13	4.86	10.37	1.67	27.74	34
Zr		92.8	7.05	30.1	50.2	8.5	97	12.77	2.60	14	14.00	11.10	189	109
Sm		2.24	2.07	1.25	5.94	0.31	13.2	1.36	1.23	1.16	1.26	1.20	4.16	7.4
Eu		0.654	0.65	0.563	1.90	0.11	4.37	0.48	0.23	0.39	0.56	0.54	1.00	2.35
Ti							1,482	4.83	405	1,253	2,157	955	4,888	2,338
Gd		2.21	1.88	2.12	5.35	0.46	9.71	1.56	0.56	1.60	2.02	1.45	2.92	4.70
Dy		2.29	1.46	2.40	3.31	0.67	7.8	1.14	0.55	1.54	2.58	1.63	2.61	3.18
Y		11.8	6.69	12.7	13.4	3.98	39	12.9	3.60	9.00	16.80	10.40	14.70	18.0
Er		1.38	0.75	1.54	1.19	0.49	3.95	1.36	0.69	1.12	1.63	1.10	1.68	1.29
Yb		1.24	0.67	1.35	1.02	0.33	3.24	0.90	0.82	0.96	1.38	0.60	1.23	0.98
Sr/Sr*		0.56	0.54	1.36	0.77	8.86	0.49	0.52	1.16	0.77	0.10	1.21	1.67	1.48
Zr/Zr*		0.28	1.07	0.87	0.23	0.24	0.03	0.40	0.03	0.40	0.22	0.50	1.13	0.47
Ti/Ti*					0.05	0.14	0.27	0.38	0.27	0.38	0.49	0.26	0.69	0.16
Y/Y*		0.85	0.90	0.60	0.91	2.19	0.72	0.90	0.72	0.90	1.04	1.02	0.92	1.13
CH														
(La/Sm)$_N$		1.13	0.73	0.73	1.81	14.95	61.01	12.47	61.01	12.47	18.05	0.30	11.72	2.47
(Sm/Dy)$_N$		2.96	0.76	1.16	2.79	1.97	3.69	1.24	3.69	1.24	0.81	1.22	2.63	3.84
(Gd/Yb)$_N$		4.23	1.13	1.41	2.43	1.41	0.55	1.39	0.55	1.39	1.18	1.95	1.91	3.87
(La/Yb)$_N$		7.07	7,13	1.12	7.07	0.73	7.91	24.17	98.21	16.67	17.66	0.65	42.44	19.95
(Eu/Eu)*		1.01	0.89	0.91	1.13	1.01	0.74	0.88	0.74	0.88	1.07	1.25	0.83	1.14

Data sources: Petrini et al. (1994), Comin-Chiaramonti et al. (2001), Lucassen et al. (2005). Primordial mantle normalized ratios, according to Sun and McDonough 1989: **PM**; chondrite normalized ratios, according to Boynton 1984: **CH**. Paraguay data, ion microprobe analyses (analytical methods in Petrini et al. 1994); Andes data, ICP-MS (analytical methods in Lucassen et al. 2005)

(2001) as the disequilibrium melting of metasomatic assemblages (dominantly amphibole) that produced carbonated silicate melts.

The geochemical discrimination among Cpx from various geodynamic mantle environment can be examined by comparing parameters as abundances and ratios of Sr, high field-strength elements as Ti and Zr, generally considered important process indicators (Rivalenti et al. 2007 and enclosed references, for a discussion). Calculated variation trends for refractory Cpx during melting of primitive mantle are shown in Fig. 14. In the Ce vs Sr diagram (Fig. 14a), the Paraguayan and Andean samples plot along the line defined by the compositional trend of the PMCE during non-modal melting (s. Johnson et al. 1990).

In particular, some Andean Cpx (e.g. A-104 sample, modal content: Ol 53.0, Opx 27.3, Cpx 17.7, Sp 3.0) display I.E. pattern (inset of Fig. 13) overlapping that of the primitive mantle (Ol 55, Opx 25, Cpx 18, Sp 2; Hofmann 1988). In the $(Sm/Yb)_N$ vs $(Ce/Nd)_N$ diagram (Fig. 14b), most Cpx compositions cluster in the quadrant III, characterized by Cpx with REE patterns having variable L- to M- to H-REE enrichment $[(Ce/Nd)_N >1; (Sm/Yb)_N > 1]$, similar to the most Cpx from xenoliths in alkali basalt from continental rift zones (Rivalenti et al. 1996 and enclosed references).

Some Cpx, straddling the quadrant III/IV boundary, could indicate a derivation from the garnet-peridotite facies either from a metasomatic component or from a pre-metasomatic Cpx. A few Cpx, plotting in quadrant I or at the I-II boundary, display U-shaped REE patterns, probably indicative of chromatographic enrichment processes. Only a few samples follow roughly the melting-related depletion trend of PMCE (Fig. 14). Most samples have Ce and Sr concentrations much higher than PMCE (Fig. 14a). This suggests open system enrichment for these elements which behave coherent in melting and open-system processes. Only one or two samples display LREE-depleted patterns expected in melting processes (Fig. 14b).

Prominent metasomatic enrichment in more refractory xenoliths (dunites and harzburgites) is evidenced by the high LREE/HREE ratio and ΣREE, which both exceed the values in lherzolites (Nielson and Noller 1987). This is consistent with higher geochemical gradients between refractory peridotites and percolating fluids. Notably, $(Ti/Zr)_N$ and $(Ti/Eu)_N$ vs $(Nd/Yb)_N$ (Fig. 14c, d) shows negative correlations, related to the relative enrichment of Zr and Eu. In particular the decoupling of Ti and Zr implies that metasomatic agents fractionated Ti-rich phases (e.g. amphibole and phlogopite) or that such phases were present in the source of the metasomatic component. The presence of such phases is consistent with both silicate and carbonate melts (Rivalenti et al. 1996).

In summary, the characteristics of trace elements are very similar in the Paraguayan and Andean samples and they overlap the compositionsl field defined by world wide xenoliths in continental basalts from continental rift zones. The variable trace elements patterns of clinopyroxenes from Paraguayan and Andean xenoliths could be the result of similar metasomatic processes at large scale which affected their trace element budget independently of previous melting-controlled major elements composition.

Given a fertile lherzolite as starting composition, the following history could be inferred:

i)   depletion by variable degrees of partial melting, as apparent from the variable major element composition ;
ii) subsolidus re-equilibration, as shown by spinel and Opx exsolution in Cpx, and subsequent variations of the V (cell) and V(M1) volumes (Princivalle et al. 2000);
iii) metasomatic processes, evidenced by variable enrichment of incompatible elements;
iv) decompression and partial melting (e.g. glassy drops in Cpx "cutting" the spinel exsolutions, blebs and glassy patches; palisade textures around Cpx), and fast ascent of the host magmas.

Sr-Nd isotopes

Sr and Nd isotopes were determined on selected whole rock (WR) samples and Cpx and Opx separates (Comin-Chiaramonti et al. 1991, 2001; Petrini et al. 1994; Lucassen et al. 2005). In the Andes the notional age of equilibrium of the lower crust xenoliths and eruption of the host lavas from Las Conchas Valley is around 100 Ma (Lucassen et al.

Fig. 12 Normalized diagrams for the clinopyroxenes from carbonatized peridotites from the Andes (Lucassen et al. 2005). PM, primordial mantle according to Sun and McDonough 1989, and chondrites, according to Boynton (1984)
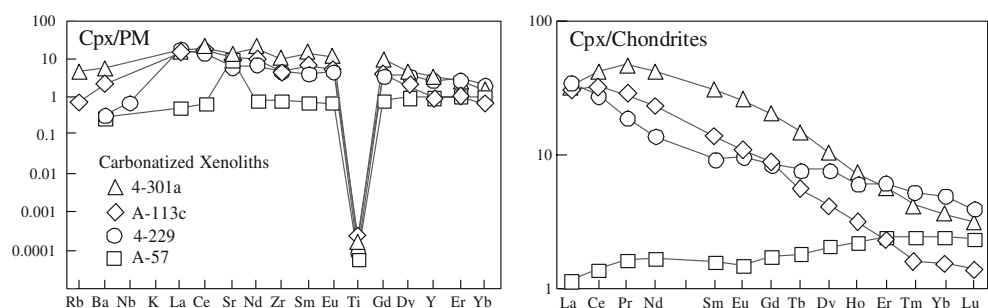
Fig. 13 Trace element and REE patterns, ion microprobe data, normalized to primitive mantle ant to chondrites, respectively, according to Hofmann (1988) and Boynton (1984) for clinopyroxene with orthopyroxene exsolutions (Paraguay-LK suite), clinopyroxene with glassy drops and the clinopyroxene coexisting with glassy patches (bleb) in the same nodule (Paraguay H-K). Data sources: Comin-Chiaramonti et al. 2001 and enclosed references
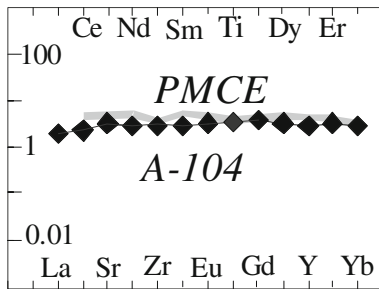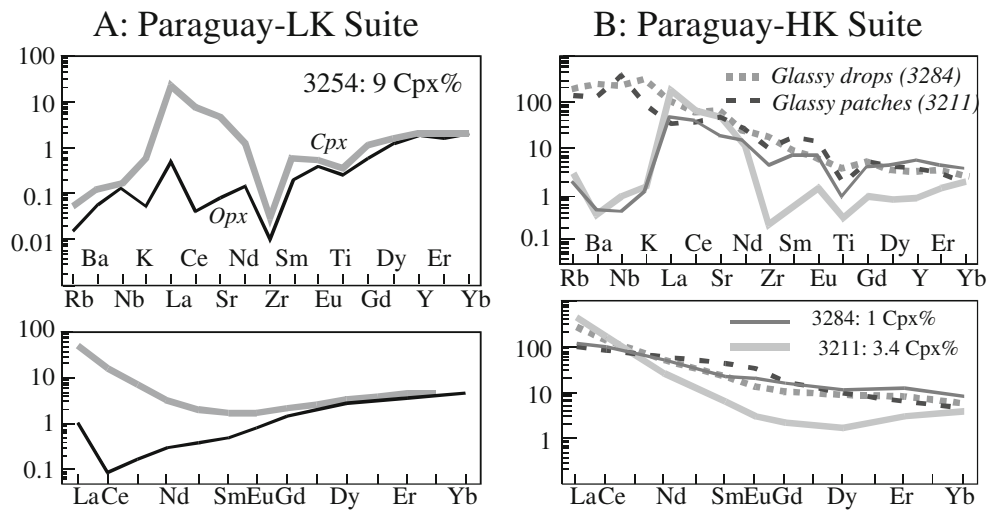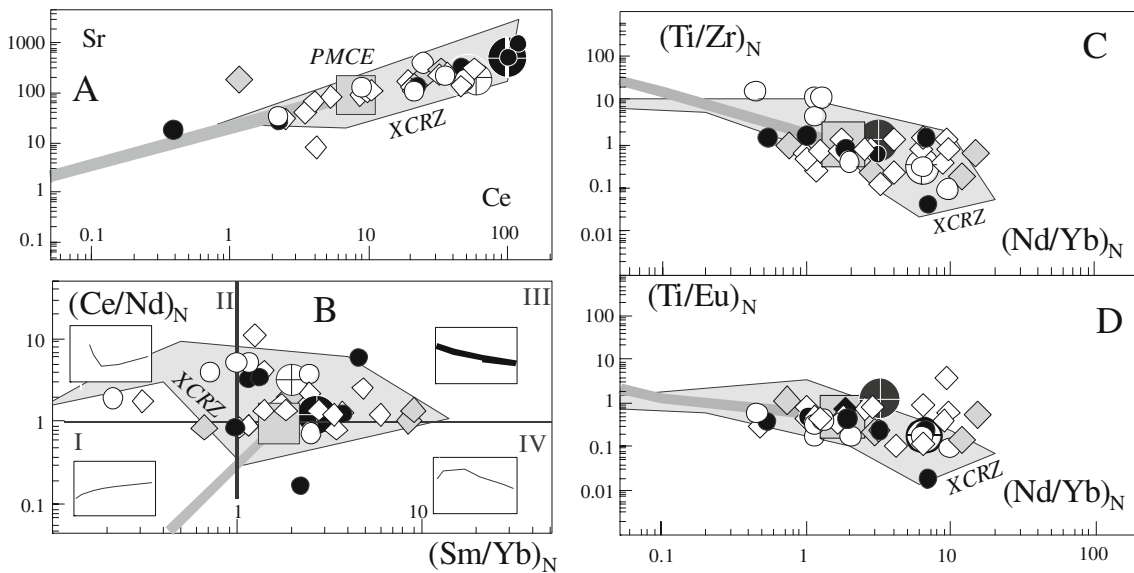
Fig. 14 Clinopyroxene compositions expressed as: **a** Ce vs Sr (ppm). PMCE: Cpx trace element composition in primitive mantle (Hofmann 1988), XCRZ, xenoliths in alkali basalts from continental rift areas. The line from PMCE in this and others panels shows the compositional trend of Cpx during fractional non-modal melting, following Johnson et al. (1990). **b** $(Ce/Nd)_N$ vs $(Sm/Yb)_N$, subdivided in four quadrants, showing the main characteristics of Cpx in terms of REE patterns: the mantle depletion, both fractional and batch models, plot in quadrant I; depleted Cpx plot in quadrant II; in quadrant III, Cpx are characterized by variable Light-, Middle- Heavy-REE negative fractionation; Cpx with REE patterns characterized by a hump at MREE plot in the IV quadrant. **c** $(Nd/Yb)_N$ vs $(Ti/Zr)_N$ and **D**: $(Nd/Yb)_N$ vs $(Ti/Zr)_N$. Normalization following Hofmann (1988). Symbols as in Fig. 8. **Inset**: I.E. and REE normalized patterns of Cpx from sample A-104 compared with the Cpx trace element in primitive mantle (cf. Fig. 12)

2005). In Asunción Province, Eastern Paraguay, an average age of 106±33 Ma (span between 132 and 61 Ma) was inferred from the alignment of the whole rock-cpx-opx and leaching solutions along a Rb-Sr errorchron (Comin-Chiaramonti et al. 2001). In the Misiones Province (age of the host lavas 118 Ma), an age of 128 Ma corresponds to the Rb-Sr errorchrone of the glassy drops in clinopryroxene (Comin-Chiaramonti et al. 2001). Therefore these reference ages were used for the calculation of the initial isotopic ratios of Cpx from mantle xenoliths of these localities.

Isotopic compositions of WR and mineral separates from Paraguay display a wide variation of initial isotope ratios, with $^{87}Sr/^{86}Sr$ overlapping in the LH and HK suites within the ranges 0.70343-0.70393 (WR) and 0.70326–0.70404 (Cpx + Opx), respectively, and $^{143}Nd/^{144}Nd$ 0.51239–0.51307 (WR) and 0.51248–0.51322 (Cpx), respectively (Fig. 15). In the Andean samples Cpx are in the ranges 0.70264–0.70498 ($^{87}Sr/^{86}$) and 0.51258–0.51310 ($^{143}Nd/^{144}Nd$), initial ratios, respectively vs. average of the host rocks initial $^{87}Sr/^{86}Sr=0.70322±0.00022$ and $^{143}Nd/^{144}Nd=0.51286±0.00028$ (Fig. 10 of Lucassen et al. 2005). It can be observe that the A-106 mantle xenolith (Cpx 7.1%) show a very strong depleted character, while the host Cpx plots inside the other analogues: this may be attributed to the fact that the enriched components affected only the clinopyroxene (s. tie line of Fig. 15).

$^{87}Rb/^{86}Sr$ ratios of the clinopyroxenes are systematically lower than those of their host rocks, and cluster between 0.0002 and 0.0086. Only one sample from LK suite and two samples from HK suite have $^{87}Rb/^{86}Sr$ ratio above 0.1 (Table 3 of Comin-Chiaramonti et al. 2001 and Table 3 of Lucassen et al. 2005).

In general, the best age fitting for $^{147}Sm/^{144}Nd$ vs $^{143}Nd/^{144}Nd$ is along a 0.5 Ga line ($r^2<0.85$; Table 4 of Comin-Chiaramonti et al. 2001). On the contrary, strongly positive correlations are shown by the clinopyroxenes from Pico Cabuji (NE Brazil; $r^2=0.99$, best fitting at 1,110 Ma) and from Fernando de Noronha ($r^2=0.90$, best fitting at 413 Ma; Fig. 6b of Comin-Chiaramonti et al. 2001).

On the other hand, in many of the Andean xenoliths the $^{147}Sm/^{144}Nd$ ratios (too low or "enriched") do not fit the observed $^{143}Nd/^{144}Nd$ (to radiogenic) ratios, and young LREE enrichment is needed in the Andean case to explain these relationships. The poor fit of $^{143}Nd/^{144}Nd$ and $^{147}Sm/^{144}Nd$ for clinopyroxenes could have variable causes, e.g. initial Nd isotope heterogeneity, variable ages or intensity of the metasomatic overprint or depletion by melt extraction. Thus, the decoupling between $^{143}Nd/^{144}Nd$ and $^{147}Sm/^{144}Nd$ ratios suggests a complex history of REE depletion and enrichment events in the mantle, as envisaged also by the trace element patterns. Finally, it is apparent in Fig. 15 that the Na-alkaline rocks from Andes roughly represent the upper extension of the Paraguay array

(Comin-Chiaramonti et al. 1997), well distinct from the Andean potassic magmatism.

Lead isotopes

Lead isotopes are available for the Cpx from Andes (Lucassen et al. 2005) and for some samples from Paraguay, both LK and HK suites (Comin-Chiaramonti and Gomes 2005). Xenoliths from both distant areas, Paraguay and the Central Andes, show similar spans of Pb isotope compositions (Fig. 16). The $^{206}Pb/^{204}Pb$, $^{207}Pb/^{204}Pb$, $^{208}Pb/^{204}Pb$ ratios vary between 17.3 and 20.6, 15.5 and 15.7, 37.5 and 41.9, respectively. Some of the samples cluster in or close to the much smaller compositional field of their host lavas and the Ayopaya carbonatite (Schultz et al. 2004). The $^{238}U/^{204}Pb$ (μ ratio) is below the typical depleted mantle value of ca. 8 for 60% of the samples, 15% show μ between 11 and 15 and 25% between 53 and 55.

Again, there is, as in the case of the Sm-Nd isotope system, a mismatch between parent/daughter ratios and the radiogenic isotope composition where a metasomatic overprint or melt extraction relatively late in the history of the lithospheric mantle is required.

In the Sr versus Pb isotopic diagrams the Andean and Paraguayan samples roughly plot into similar fields between EMI, DMM and HIMU mantle end members (Fig. 16; Zindler and Hart 1986). Nd isotope ratios of many Andean xenoliths are more radiogenic than in Paraguayan samples (Fig. 16), suggesting a higher 'more depleted' $^{147}Sm/^{144}Nd$ during a prolonged period in the Andean mantle. Compositions of Andean and Paraguayan xenoliths show a broad variability with respect to mantle end-member compositions (Fig. 16), which is not explained by mixing of two uniform sources, e.g. a uniform lithisopheric mantle and the relatively uniform host lavas. The compositional variety could be explained (1) by metasomatic addition of materials with different Nd and Sr isotopic composition and variable inheritance of thorogenic Pb from the pre-Cretaceous evolution of the upper mantle or (2) by metasomatic changes in the Sm/Nd, Rb/Sr, U/Pb, Th/Pb ratios in the respective sample volumes and longterm separation from melting, or further metasomatism (Lucassen et al. 2005 for a discussion). The isotope signatures of xenoliths from boths regions require metasomatism in the mantle and long-term separation from melting and convection whatever the process of introduction of the specific isotope signature to the respective sample.

Discussion and concluding remarks

Na-alkali magmatism is subordinate in Paraguay (late Lower Cretaceous to Eocene) but dominant in the Andes
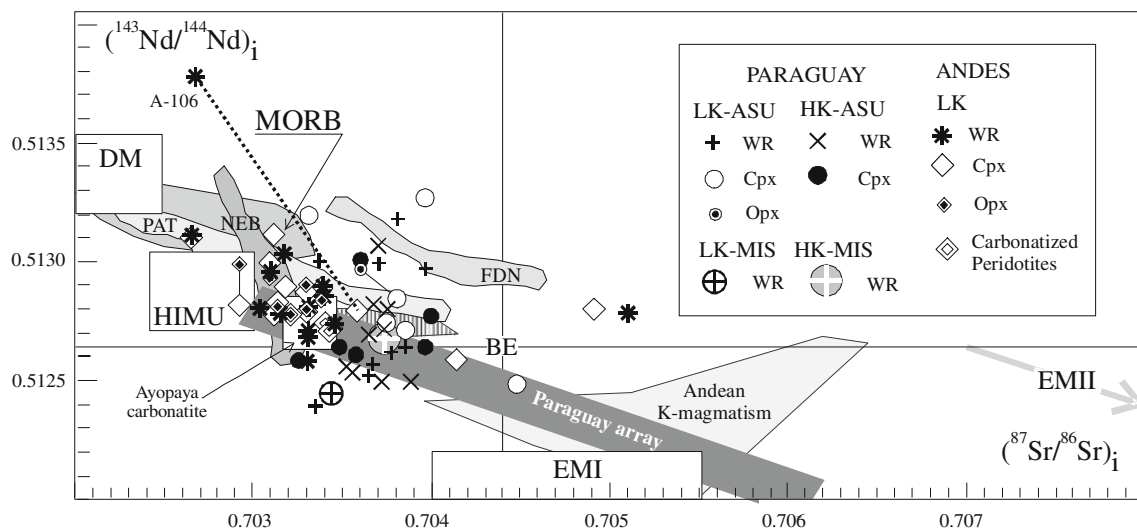
Fig. 15 $^{87}Sr/^{86}Sr$ vs $^{143}Nd/^{144}Nd$ plot for Paraguay and Andes clinopyroxenes and host xenoliths. For comparison the compositional fields of Cpx from NE Brazil (NEB), Fernando de Noronha (FDN; Rivalenti et al. 2000), Patagonia (PAT, Barbieri et al. 1997) and Andean potassic magmatism (Lucassen et al. 2007) are also plotted. Dotted line joins the more depleted xenolith (A-106) with the hosted Cpx. Data source: Comin-Chiaramonti and Gomes (2005), Comin-Chiaramonti et al. (1991, 2001), Lucassen et al. (2005, Fig. 10); Ayopaya carbonatite: Schultz et al. (2004). Paraguay array represents the trend of Cretaceous to Paleogene volcanics in Paraguay (after Comin-Chiaramonti et al. 1997). The dashed field represents the sodic alkaline mafic rock types from Andes

(Cretaceous) at ~26°S. These mafic-ultramafic rocks display similar bulk compositions and trace element patterns at both localities, including the positive Nb, Ta and Ba spikes and negative K anomalies (Comin-Chiaramonti et al. 2007; Lucassen et al. 2007). The main difference between Paraguayan and Andean Na-magmatism is a higher Rb concentration in the Paraguayan samples. Sr-Nd-Pb isotopic features are also very similar and most of the samples follow a DMM-EMI trend with a high-μ component, i.e. radiogenic Pb component in the Andean lavas. According to Comin-Chiaramonti et al. (1997, 2001) the volcanic suites derive from 4 to 6% melting of a garnet-peridotite source.

Mantle xenoliths of spinel peridotite facies from similar latitudes in the Andes and Paraguay crystallized at similar temperatures and pressures. They apparently follow in the P-T diagram a common geotherm starting at about 830°C and 10Kb and intersecting the hydrous peridotite solidus at about 1,140°C and 21–22 Kb. Both suites are variable in their major element compositions, ranging from "fertile" to very depleted in "basaltic component". Two suites can be distinguished: low and high in K_2O content ($K_2O < 0.1$ and > 0.1, LK and HK, respectively). The HK suite is restricted to xenoliths from Paraguay and some of these have exceedingly high K_2O and incompatible elements compared with the composition of peridotites which underwent partial melting during basalt-extraction (Frey and Green 1974). The major element contents of the xenoliths and the compositional variations of mineral phases are largely consistent with residual compositions after variable degrees of partial melting, but metasomatic effects are apparent

especially in the HK suite (De Marchi et al. 1988; Petrini et al. 1994, Lucassen et al. 2005). De Marchi et al. (1988) have shown that K is mostly partioned into glassy patches (blebs) in the xenoliths and into glassy drops in the clinopyroxenes.

Variable trace element enrichment in Paraguayan and Andean xenoliths also suggests that processes other than depletion played an important role in the mantle. I.E. variability is largely decoupled from major element composition of the xenoliths, which is also common in other xenoliths suites worldwide and broadly linked to metasomatic processes involving fluids and/or small volume melts (Menzies et al. 1985; Erlank et al. 1987). The I.E. content of clinopyroxenes from LK and HK is highly variable, similar to other world-wide occurrences (Salters and Shimizu 1988). The REE enrichment is most variable in Cpx with spongy texture and abundant glassy drops (eg. sample 3284; Table 4). A possible explanation for the progressive enrichment of samples characterized by similar HREE and different LREE abundances is different ion-exchange processes ("simple mixing metasomatism model" of Song and Frey 1989; Sen et al. 1993), due to the passage of LREE-rich chemical front on depleted compositions, both in LK and HK suites. Trace elements geochemistry excludes contamination of xenoliths and blebs by their enclosing lavas. Nb, Ta and Ba display positive and K negative anomalies in the lavas, whereas in the xenoliths and blebs these elements show opposite patterns and ratios between these and other incompatible elements are very distinct in lavas and xenoliths.

Fig. 16 Sr, Nd and Pb isotopic composition of clinopyroxene separates of mantle xenoliths from the Andes and Paraguay. Grey field: host lavas. Data sources as in Table 3. Symbols as in Fig. 15. DMM, HIMU and EMI components after Zindler and Hart (1986), Hart and Zindler (1989). Crystalline basement as in Comin-Chiaramonti and Gomes (2005). For comparison the Ayopaya carbonatite is also plotted (Schultz et al. 2004)
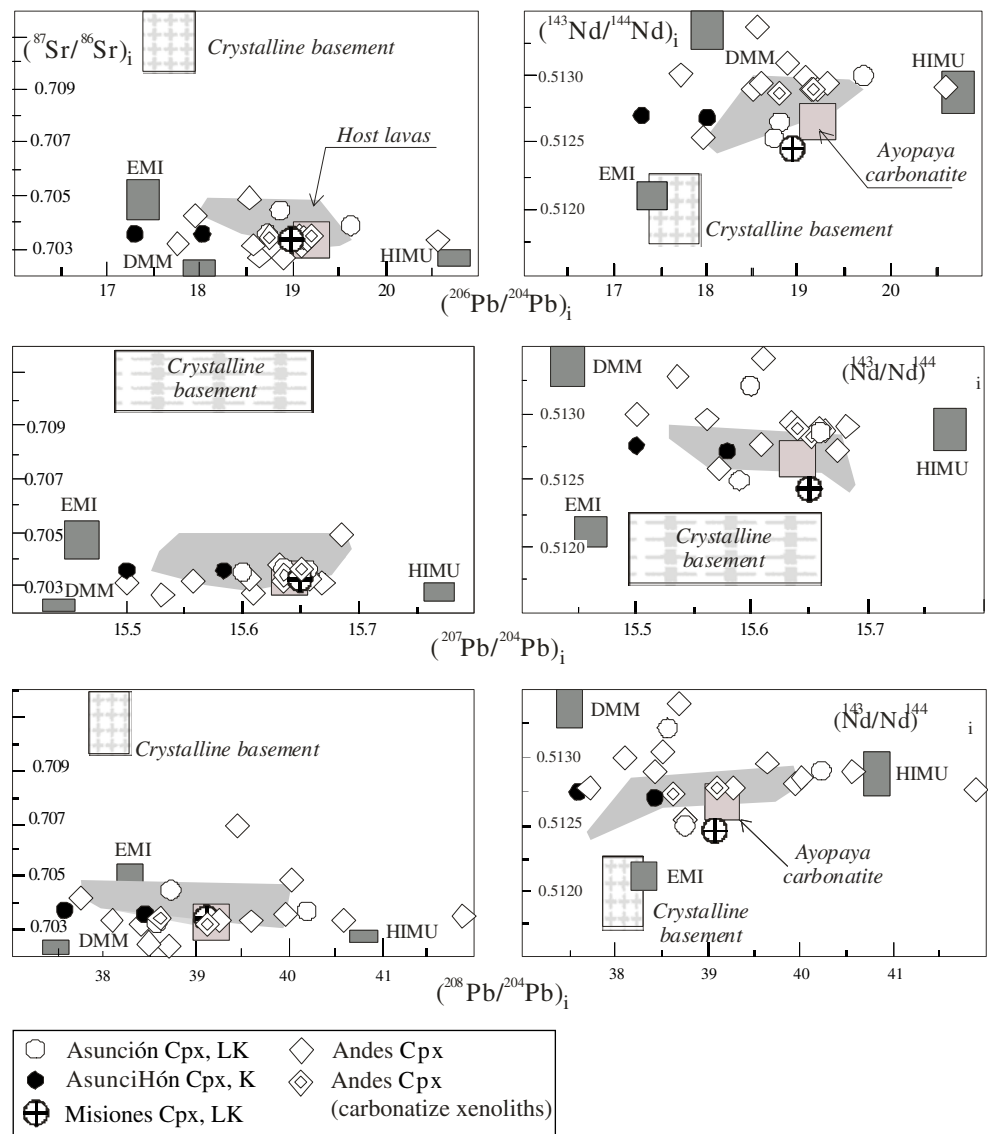
Radiogenic isotope compositions of the two xenoliths suites and their host rocks show considerable overlap, i.e. their composition can be described by the same set of mantle "mantle end members". As expected for the small sample volumes, the compositional range in the xenoliths is larger than in their host lavas (Figs. 15 and 16). Oxygen isotope composition of cpx and opx from both suites is very similar (Table 3).

A tentative link between the geotectonic setting and the metasomatism in the lithospheric mantle is outlined in the following. Subduction is accepted as a first order process at this margin from Neoproterozoic onwards, regardless the concepts and details of the tectonic evolution inferred from different data sets and working groups (e.g. Ramos and Aleman 2000; Scheuber and González 1999; Taylor et al. 2005; Oliveiros et al. 2007; Ramos 2008). Therefore it is reasonable to relate the origin of the metasomatic fluids that impregnated the Andean xenoliths to the subduction of an oceanic slab below the peridotite wedge. Fluids and/or small melt fractions from the slab induce LILE and LREE enrichment and Nb-Ta retention from rutiles of the slab eclogites (e.g. Rivalenti et al. 1998, Leitch and Davis 2001). Small amounts of rutile (~2%) are sufficient to prevent HSFE enrichment in the mantle wedge (Rivalenti et al. 1998 and enclosed references).

The intensity and distribution of the enrichment due the interaction of slab fluids and wedge can vary depending on several factors as thickness and permeability of the mantle wedge and depth of the subducted slab. The age of such metasomatism in the xenoliths is uncertain. It is reasonable to link the metasomatic imprint on the xenoliths to subduction, but the knowledge of the age would be crucial to link mantle-metasomatism to a certain tectonic event. Lucassen et al. (2005) proposed an Early Paleozoic component in the lithospheric mantle of the Andean xenoliths in order to explain the radiogenic Pb in the

intraplate magmatic rocks by in-situ growth from elevated U/Pb ratios, without invoking high-μ plume sources, which are unlikely in this longstanding active margin setting.

In Paraguay, xenoliths and host lavas outcrop close to crystalline rocks of the Caapucú High, the northwestern part of the Rio de La Plata Craton (Fulfaro 1996). According to Dalla Salda et al. (1992) a plutonic (magmatic?) arc setting in this region would be possible only in late Paleoproterozoic times. The Rio de La Plata Craton is stable since Early Proterozoic times. The origin of the metasomatic material could be related to volatile rich fluids derived from partial molten diapirs from depths less than 200 km (Comin-Chiaramonti et al. 1991). Sr-Nd isotopic data on 1.8 Ga tholeiites from the Rio de La Plata Craton indicate that the mantle source is composed by a depleted end-member strongly contaminated by an EMI component (Girardi 2006). Paraguayan lavas and enclosed xenoliths could have a component of inherited isotopic characteristics from the Paleoproterozoic evolution. Such old compositional features in the lithospheric mantle could be activated by decompression melting and percolation of melts and fluids in the mantle during Cretaceous to Paleogene mantle-derived intraplate magmatism. This magmatism, which also brought the xenolith to the surface, would provide the minimum age for metasomatism seen in the radiogenic isotope systems from an external source. Neoproterozoic — Early Palaoeozoic influence from possible rifting-subduction is another option for the Paraguyan samples, if the proposed rifting and closure of the Puncoviscana basin (at the eastern edge of the Early Paleozoic reworked basement in Fig. 1a; e.g. Omarini et al. 1999) or the Cambrian accretion of a Laurentia derived terrane (AAB and PA in Fig. 1; Rapela et al. 2007) is considered. A timely relatively close subduction related metasomatism in the lithospheric mantle of the Andean and Paraguayan sections would be feasible considering these scenarios for the Neoproterozoic — Early Paleozoic or the release of material from already deeply subducted oceanic crust in a situation similar to the present (Fig. 1b).

Such old compositional features in the lithospheric mantle could be activated by decompression melting and percolation of melts and fluids in the mantle during Cretaceous to Paleogene mantle-derived intraplate magmatism. This magmatism, which also brought the xenolith to the surface, would provide the minimum age for metasomatism seen in the radiogenic isotope systems from an external source. Whatever the model or age for metasomatism in the xenoliths (in the case of the radiogenic isotopes external young metasomatism or internal radiogenic growth after old metasomatism), a source with elevated U/Pb and Rb/Sr, well above the MORB-type depleted mantle is needed. This source has to be long-term separated from melting or the convective mantle.

Finally, we stress that the compositional characteristics of mantle xenoliths and host sodic alkaline lavas are surprisingly similar at about 26°S in the extensional intra-plate setting (Paraguay) and in the Cretaceous to Tertiary Andean extensional system, which parallels the back-arc.

References

Barbieri MA, Rivalenti G, Cingolani C, Mazzucchelli M, Zanetti A (1997) Geochemical and isotope variability of the northern and southern Patagonia lithospheric mantle (Argentina). Proceedings of South America Symposiumon Isotope Geology, Campos do Jordão, São Paulo, Brazil, Extended Abstract: 41–43

Bonatti E, Michael J (1989) Mantle peridotites from continental rifts to ocean basins to subduction zones. Earth Plan Sci Lett 91:297–311

Boynton WV (1984) Cosmochemistry of the rare earth elements: meteorite studies. In: Henderson P (ed) Rare Earth Element geochemistry. Elsevier, Amsterdam, pp 63–114

Brey GP, Köhler T, Nickel KG (1990) Geothermobarometry in four-phase Lherzolites I. Experimental results from 10 to 60 kb. J Petrol 31:1313–1352

Bristow JF (1984) Nephelinites of the North Lebombo and South East Zimbawe. Spec Publ Geol Soc South Africa 13:87–104

Chaffey DJ, Cliff RA, Wilson BM (1989) Characterization of the St Helena magma source. In: Sunders D & Norry MS (eds) Magmatism in the Ocean basin. Geol. Society, Special Paper 42: 257–276.

Chiba H, Chack T, Clayton RN, Goldsmith J (1989) Oxygen isotope fractionations involving diopside, forsterite, magnetite, and calcite: Application to geothermometry. Geochim Cosmochim Acta 53:2985–2995

Comin-Chiaramonti P, Gomes CB (1996) Alkaline Magmatism in Central-Eastern Paraguay. Relationships with coeval magmatism in Brazil. Edusp/Fapesp, São Paulo, Brazil, p 464

Comin-Chiaramonti P, Gomes CB (2005) Mesozoic to Cenozoic alkaline magmatism in the Brazilian Platform. Edusp/Fapesp, São Paulo, Brazil, p 752

Comin-Chiaramonti P, Demarchi G, Girardi VAV, Princivalle F, Sinigoi S (1986) Evidence of mantle metasomatism and heterogeneity from peridotite inclusions of northeastern Brazil and Paraguay. Earth Plan Sci Lett 77:203–217

Comin-Chiaramonti P, Civetta L, Petrini R, Piccirillo EM, Bellieni G, Censi P, Bitschene P, DeMarchi G, De Min A, Gomes CB, Castillo AMC, Velázquez JC (1991) Cenozoic nephelinitic magmatism in Eastern Paraguay: petrology, Sr-Nd isotopes and genetic relationships with associated spinel-peridotite xenoliths. Europ J Mineral 3:507–525

Comin-Chiaramonti P, Cundari A, Piccirillo EM, Gomes CB, Castorina F, Censi P, De Min A, Marzoli A, Speziale S, Velázquez VF (1997) Potassic and sodic igneous rocks from Eastern Paraguay: their origin from the lithospheric mantle and genetic relationships with the associated Paraná flood tholeiites. J Petrol 38:495–528

Comin-Chiaramonti P, Princivalle F, Girardi VAA, Gomes CB, Laurora A, Zanetti F (2001) Mantle xenoliths from Ñemby, Eastern Paraguay: O-Sr-Nd isotopes, trace elements and crystal chemistry of hosted clinopyroxenes. Periodico di Mineralogia 70:205–230

Comin-Chiaramonti P, Marzoli A, Gomes CB et al (2007) Origin of Post-Paleozoic magmatism in Eastern Paraguay. In: RG Foulger and DM Jurdy (eds) The origin of melting anomalies. Geological Society of America, Special Paper 430, pp. 603–633

Dalla Salda LH, Francese JR, Posadas VG (1992) The 1800 Ma mylonite-anatectic granitoid association in Tandilia, Argentina. Basement Tec 7:161–174

De La Roche H (1986) Classification et nomenclature des roches ignées: un essai de restauration de la convergence entre systématique quantitative, typologie de l'usage et modélisation génétique. Bull Soc Géol de France 8:337–353

De Marchi G, Comin-Chiaramonti P, De Vito P, Sinigoi S, Castillo AMC (1988) Lherzolite-dunite xenoliths from Eastern Paraguay: petrological constraints to mantle metasomatism. In: Piccirillo EM, Melfi AJ (eds) The Mesozoic Flood Volcanism from the Paraná Basin (Brazil). Petrogenetic and geophysical aspects. Iag-Usp, São Paulo, Brazil, pp 207–227

Erlank AJ, Waters FG, Hawkesworth CJ et al (1987) Evidence for mantle metasomatism in peridotite nodules from the Kimberley pipes, South Africa. In: Menzies ML, Hawkesworth CJ (eds) Mantle metasomatism. Academic, London, pp 221–311

Fabriès J (1979) Spinel-olivine geothermometry in peridotites from ultramafic complexes. Contrib Mineral Petrol 69:329–336

Franz G, Lucassen F, Kramer W et al (2006) Crustal evolution at the Central Andean continental margin: a geochemical record of crustal growth, recycling and destruction. In: Oncken O, Chong G, Franz G et al (eds) The Andes: Active Subduction Orogeny. Frontiers in Earth Sciences, 1. Springer Verlag, Heidelberg, pp 45–64

Frey FA, Green DH (1974) The mineralogy, geochemistry and origin of lherzolite inclusions in Victorian basanites. Geoch Cosmochim Acta 38:1023–1050

Fulfaro V (1996) Geology of Eastern Paraguay. In: Comin-Chiaramonti P, Gomes CB (eds) Alkali magmatism in Central Eastern Paraguay. Brazil, Edusp/Fapesp, pp 17–31

Gibson SA, Thompson RN, Day JA (2006) Timescales and mechanism of plume-lithosphere interaction: $^{40}Ar/^{39}Ar$ geochronology and geochemistry of alkaline igneous rocks from the Paraná-Etendeka large igneous province. Earth Plan Sci Lett 251:1–17

Girardi VAV (2006) Sr-Nd isotopic study of selected Paleo- and Mesoproterozoic mafic intrusions from cratonic areas of Brazil and Uruguay: inferences on their mantle sources. V South American Symposium on Isotope Geology- Uruguay, Short papers, pp. 378–381

Gregoire M, Tinguely C, Bell DR, Le Roex AP (2005) Spinel lherzolite xenoliths from the Premier kimberlite (Kaapvaal craton, South Africa): nature and evolution of the shallow upper mantle beneath the Bushveld complex. Lithos 84:185–205

Hart SR, Zindler A (1989) Constraints on the nature and the development of chemical heterogeneities in the mantle. In: Peltier WR (ed) Mantle convection plate tectonics and global dynamics. Gordon and Breach Sciences Publishers, New York, pp 261–388

Hauri EH (1997) Melt migration and mantle chromatography, I: simplified theory and conditions for chemical and isotopic decoupling. Earth Plan Sci Lett 153:1–19

Hirschmann M (2000) Mantle solidus: experimental constraints and the effects of peridotite composition. Geochem Geophys Geosyst 1(10):1042

Hofmann AW (1988) Chemical differentiation of the Earth: the relationship between mantle, continental crust and oceanic crust. Earth Plan Sci Lett 153:1–19

Johnson KTM, Dick HJB, Shimizu N (1990) Melting in oceanic upper mantle: an ion microprobe study of diopsides in abyssal peridotites. J Geophys Res 95:2661–2678

Keller J, Hoefs J (1995) Stable isotope characteristics of recent natrocarbonatites from Oldoinyo Lengai. In: Bell K, Keller J (eds) Carbonatite volcanism: Oldoiynio Lengai and the petrogenesis of natrocarbonatites. Springer, Berlin, pp 113–123

Kyser TK (1990) Stable isotopes in the continental lithospheric mantle. In: Menzies MA (ed) Continental mantle. Clarendon, Oxford, pp 127–156

Kyser TK, O'Neil JR, Carmichael ISE (1981) Oxygen isotope thermometry of basic lavas and mantle nodules. Contrib Mineral Petrol 77:11–23

Laurora A, Mazzucchelli M, Rivalenti G et al (2001) Metasomatism and melting in carbonated peridotite xenoliths from the mantle wedge: the Gobernador Gregore case (Southern Patagonia). J Petrol 42:69–87

Leitch AM, Davis GF (2001) Mantle plumes and flood basalts: enhanced melting from plume ascent and an eclogite component. J Geophys Res 106:2047–2059

Le Maitre RW (1989) A classification of igneous rocks and glossary of terms. Blackwell Scientific Publications, Oxford, p 193

Lucassen F, Becchio R, Wilke HG et al (2000) Proterozoic– Paleozoic development of the basement of the Central Andes (18°-26°)–a mobile belt of the South American craton. J South Am Earth Sci 13:697–715

Lucassen F, Escayola M, Franz G, Romer RL, Koch K (2002) Isotopic composition of late Mesozoic basic and ultrabasic rocks from Andes, 23–32º S)–implications for the Andean mantle. Contrib Mineral Petrol 143:336–349

Lucassen F, Franz G, Viramonte J, Romer RL, Dulski P, Lang A (2005) The late Cretaceous lithospheric mantle beneath the Central Andes: evidence from phase equilibrium and composition of mantle xenoliths. Lithos 82:379–406

Lucassen F, Franz G, Romer RL, Schultz F, Dulski P, Wemmer K (2007) Pre-Cenozoic intra-plate magmatism along the Central Andes (17–34°S): Composition of the mantle at an active margin. Lithos 99:312–338

MacRae NE (1979) Silicate glass and sulfides in ultramafic xenoliths, Newer basalts, Victoria, Australia. Contrib Mineral Petrol 68:275–280

McKenzie D, O'Nions RK (1991) Partial melt distributions from inversion of rare earth element concentrations. J Petrol 32:1021–1091

Menzies MA, Hawkesworth CJ (1987) Mantle Metasomatism. Academic, Geology Series, London, p 453

Menzies MA, Kempton P, Dungan M (1985) Interaction of continental lithosphere and asthenospheric melts below the Geronimo volcanic field, Arizona. J Petrol 26:663–693

Menzies MA, Rogers N, Tindle A, Hawkesworth CJ (1987) Metasomatic and enrichment processes in lithospheric perido-tites, an effect of asthenosphere-lithosphere interaction. In: Menzies MA, Hawkesworth CJ (eds) Mantle Metasomatism. Academic, Geology Series, London, pp 313–364

Mercier JC (1980) Single-pyroxene geothermometry and geobarometry. Am J Sci 61:603–615

Mercier JC, Benoit V, Girardeau J (1984) Equilibrium state of diopside-bearing harzburgites from ophiolites: geobarometric and geodynamic implications. Contrib Mineral Petrol 85:391–403

Moore AE, Blenkinsop TG, Cotterill F (2008) Controls on post-Gondwana alkaline volcanism in Southern Africa. Earth Planet Sci Lett 268:151–164

Morimoto N (1989) Nomenclature of pyroxenes. Can Mineral 27:143–156

Nielson JE, Noller JS (1987) Processes of mantle metasomatism; constraints from observations of composite mantle xenoliths. Geol Soc of America, S.P. 215:61–75

Nimis P (1995) A clinopyroxene geobarometer for basaltic systems based on crystal-structure modelling. Contrib Mineral Petrol 121:115–125

O'Reilly SY, Griffin WC (1988) Mantle metasomatism beneath western Victoria, Australia. 1: Metasomatic processes in Cr diopside lherzolites. Geochim Cosmochim Acta 52:433–448

Oliveiros V, Morata D, Aguirre L, Féraud G, Fornari M (2007) Jurassic to Early Cretaceous subduction-related magmatism in the Coastal Cordillera of northern Chile (18°30'–24°S): geochemistry and petrogenesis. Rev Geol de Chile 34:209–232

Omarini R, Sureda RJ, Gotze HJ, Seilacher A, Pfluger F (1999) Puncoviscana folded belt in northwestern Argentina: testimony of late Proterozoic Rodinia fragmentation and pre-Gondwana collisional episodes. Intern J Earth Sci 88:76–97

Perkins G, Zachary S, Serverstone J (2006) Oxygen isotope evidence for subduction and rift-related mantle metasomatism beneath the Colorado Plateau-Rio Grande rift transition. Contrib Mineral Petrol 151:633–650

Petrini R, Comin-Chiaramonti P, Vannucci R (1994) Evolution of the lithosphere beneath Eastern Paraguay: geochemical evidence from mantle xenoliths in the Asunción-Ñemby nephelinites. Mineral Petrographica Acta 37:247–259

Piccirillo EM, Melfi AJ (1988) The Mesozoic Flood Volcanism from the Paraná Basin (Brazil). Petrogenetic and geophysical aspects. Iag-Usp, São Paulo, Brazil, p 600

Princivalle F, Tirone M, Comin-Chiaramonti P (2000) Clinopyroxenes from metasomatized spinel-peridotite mantle xenoliths from Ñemby (Paraguay): crystal chemistry and petrological implications. Mineral Petrol 70:25–35

Rampone E, Bottazzi P, Ottolini L (1991) Complementary Ti and Zr anomalies in orthopyroxene and clinopyroxene from mantle peridotites. Nature 354:518–521

Ramos VA (2008) The basement of the central Andes: the Arequipa and related terranes. Ann Rev Earth Planet Sci 36:289–324

Ramos VA, Aleman A (2000) Tectonic evolution of Andes. In: Cordani UG, Milani EJ, Thomas Filho A, Campos DA (Eds) Tectonic evolution of South America. 31° International Geological Congress, Rio de Janeiro, pp 635–688

Rapela CW, Pankhurst RJ, Casquet C et al (2007) The Río de la Plata craton and the assembly of SW Gondwana. Earth-Sci Rev 83:49–82

Rivalenti G, Vannucci R, Rampone E et al (1996) Peridotite clinopyroxene chemistry reflects mantle processes rather than continental versus oceanic settings. Earth Plan Sci Lett 139:423–437

Rivalenti G, Mazzucchelli M, Girardi VAV et al (1998) Petrogenesis of the Paleoproterozoic basalt–andesite–rhyolite dyke association in the Carajas region, Amazonian craton. Lithos 43:235–265

Rivalenti G, Mazzucchelli M, Girardi VAV et al (2000) Composition and processes of the mantle lithosphere in northeastern Brazil and Fernando de Noronha: evidence from mantle xenoliths. Contrib Mineral Petrol 138:308–325

Rivalenti G, Mazzucchelli M, Zanetti A et al (2007) Xenoliths from Cerro de los Chenques (Patagonia): an example of slab-related metasomatism in the backarc lithospheric mantle. Lithos 99:45–67

Roden MF, Frey FA, Francis DM (1984) An example of consequent mantle metasomatism in peridotite inclusions from Nunivak Island, Alaska. J Petrol 25:546–577

Salters VJM, Shimizu N (1988) World-wide occurrence of HFSE-depleted mantle. Geochim Cosmochim Acta 52:2177–2182

Scheuber E, González G (1999) Tectonics of the Jurassic-Early Cretaceous magmatic arc of the north Chilean Coastal Cordillera (22°–26°S): a story of crustal deformation along a convergent plate boundary. Tectonics 18:895–910

Schultz F, Lehmann B, Tawackoli S, Rössling R, Belyatsky B, Dulski P (2004) Carbonatite diversity in the Central Andes: the Ayopaya alkaline province, Bolivia. Contrib Mineral Petrol 148:391–408

Sen G, Frey FA, Shimizu N, Leeman WP (1993) Evolution of the lithosphere beneath Oahu, Hawaii: rare earth element abundances in mantle xenoliths. Earth Plan Sci Lett 119:53–69

Shaw CS, Klügel A (2002) The pressure and temperature conditions and timing of glass formation in mantle-derived xenoliths from Baarley, West Eifel Germany: the case for amphibole breakdown, lava infiltration and mineral-melt reaction. Mineral Petrol 74:163–187

Song Y, Frey FA (1989) Geochemistry of peridotite xenoliths in basalts from Hannuoba, eastern China: implications for subcontinental mantle heterogeneity. Geochim Cosmoch Acta 53:97–113

Spera FJ (1984) Carbon ioxide in petrogenesis. III: role of volatiles in the ascent of alkaline-bearing magmas with special reference to xenolith-bearing mafic lavas. Contrib Mineral Petrol 88:217–232

Speziale S, Censi P, Comin-Chiaramonti P, Ruberti E, Gomes CB (1997) Oxygen and Carbon isotopes in the Barra do Itapirapuã and Mato Preto carbonatites (southern Brazil). Mineral Petrographica Acta 40:1–21

Sun SS, McDonough WF (1989) Chemical and isotopic systematics of oceanic basalts. In: Saunders D, Norry MJ (eds) Magmatism in the ocean basins. Geol. Society, Special Paper 42: 313–345

Taylor GK, Dashwood B, Grocott J (2005) Central Andean rotation pattern: evidence from paleomagnetic rotations of an anomalous domain in the forearc of northern Chile. Geology 33:777–780

Velázquez VF, Comin-Chiaramonti P, Cundari A, Gomes CB, Riccomini C (2006) Cretaceous Na-alkaline magmatism from Misiones province (Paraguay): relationships with the Paleogene Na-alkaline analogue from Asunción and geodynamic significance. J Geology 114:593–614

Viramonte JG, Kay SM, Becchio R, Escayola M, Novitski I (1999) Cretaceous rift related magmatism in central-western South America. J South Am Earth Sci 12:109–121

Wang J, Hattori KH, Kilian R, Stern CR (2007) Metasomatism of sub-arc peridotites below southermost South America: reduction of fO2 by slab-melt. Contrib Mineral Petrol 153:607–624

Wells PRA (1977) Pyroxene thermometry in simple and complex systems. Contrib Mineral Petrol 42:109–121

Zindler A, Hart SR (1986) Chemical geodynamics. Annu Rev Earth Planet Sci 14:493–571